Linearized 2.5-D parameter imaging-inversion in anisotropic elastic media

Stig-Kyrre Foss[1], Maarten V. de Hoop[2] and Bjørn Ursin[3]

[1] *Institute of Mathematics, NTNU, Trondheim, Norway.*
[2] *Center for Wave Phenomena, Colorado School of Mines, Golden CO 80401-1887, USA*
[3] *Institute of Petroleum Technology, NTNU, Trondheim, Norway.*

ABSTRACT

In this paper we derive 2.5-D high frequency modelling and imaging-inversion formulas of seismic reflection data in the Born approximation in anisotropic elastic media. The 2.5-D approach encompasses 3-D wave scattering measured in a common azimuth acquisition geometry subject to 2-D dimensional computations under appropriate assumptions. The lowest possible symmetry of the medium in this approach, in principle, is monoclinic, while the medium must be translationally invariant in the normal direction to the associated symmetry plane. In the presence of caustics, artifacts may be generated by the imaging-inversion procedures. We show that in the 2.5-D approach the analysis of artifacts in the 2-D symmetry plane implies the corresponding analysis in 3-D in the framework of the common azimuth acquisition geometry. An interesting aspect of our results is the occurrence of out-of-plane geometrical spreading in the least-squares removal of the contrast source radiation patterns on the data. We finally introduce the 2.5-D transform that generates common image-point gathers. This transform yields an efficient, though in general, approximate tool for migration velocity analysis in anisotropic media. A real ocean bottom seismic data example from the North Sea, using the derived formulas, is given.

Key words: Reflection seismology, seismic modelling, inversion, ray theory, anisotropy.

SYMBOLS AND NOTATION

Symbols	Description
t	time
ω	angular frequency
$\boldsymbol{x} = (x_1, x_3)(= (x_1, x_2, x_3))$	position vector (before redefi nition in main text)
$G_{in}(\boldsymbol{x}^r, \omega, \boldsymbol{x}^s)$	Green's function in the frequency domain
$\boldsymbol{x}^s, \boldsymbol{x}^r$	source and receiver positions
$A(\boldsymbol{x}, \boldsymbol{x}^s)$	amplitude for a ray at $\boldsymbol{x}^s$ from $\boldsymbol{x}$
$\mathbf{h} = (h_1, h_2, h_3)$	polarization vector
$T(\boldsymbol{x}, \boldsymbol{x}^s)$	traveltime for a ray between $\boldsymbol{x}$ and $\boldsymbol{x}^s$
$\kappa(\boldsymbol{x}, \boldsymbol{x}^s)$	KMAH index for a ray between $\boldsymbol{x}$ and $\boldsymbol{x}^s$
$v(\boldsymbol{x})$	phase velocity
$\rho(\boldsymbol{x}) = \rho^{(0)}(\boldsymbol{x}) + \rho^{(1)}(\boldsymbol{x})$	density as a sum of a smoothly varying term and a perturbation
$c_{ijkl}(\boldsymbol{x})$ $= c^{(0)}_{ijkl}(\boldsymbol{x}) + c^{(1)}_{ijkl}(\boldsymbol{x})$	elastic stiffness tensor as a sum of smooth background parameters and a perturbation
$\det\ \mathbf{Q}_2(\boldsymbol{x}, \boldsymbol{x}^s)$	relative geometrical spreading in local surface coordinates on the wavefront
$Q_2^{\|\|}(\boldsymbol{x}, \boldsymbol{x}^s)$	in-plane relative geometrical spreading
$Q_2^{\perp}(\boldsymbol{x}, \boldsymbol{x}^s)$	out-of-plane relative geometrical spreading
(q_1, q_2)	local wavefront coordinates
$\mathbf{p} = (p_1, p_2, p_3)$	slowness vector

$\boldsymbol{p}^s, \boldsymbol{p}^r$	slowness vector at at scattering point of the ray from the source and the receiver, respectively
$\mathbf{V} = (V_1, V_2, V_3)$	group velocity vector
$\hat{n}$	normal to slowness surface
$u_{mn}(\boldsymbol{x}^r, t, \boldsymbol{x}^s)$,	scattered field in time
$U_{mn}(\boldsymbol{x}^r, \omega, \boldsymbol{x}^s)$	scattered field in frequency
$\mathbf{L}$	modelling operator
$X \subset \mathbb{R}^2$	open subset in plane of consideration
$\Sigma \subset \partial X \times \partial X$	acquisition lines
$Y = \Sigma \times \mathbb{R}_{\geq 0}$	acquisition manifold
$D \subset \Sigma \times X$	open subset per branch in case of triclicated wavefields
$T(\boldsymbol{x}^r, \boldsymbol{x}, \boldsymbol{x}^s)$	two-way traveltime
$A^{\vert\vert}(\boldsymbol{x}, \boldsymbol{x}^s)$	GRA amplitude with only in-plane geometrical spreading
$\mathcal{L}_R^{\perp}(\boldsymbol{x}^r, \boldsymbol{x}, \boldsymbol{x}^s)$	total out-of-plane geometrical spreading
$\mathbf{w}(\boldsymbol{x}^r, \boldsymbol{x}, \boldsymbol{x}^s)$	radiation patterns 'vector'
$\mathbf{c}^{(1)}(\boldsymbol{x})$	medium parameter perturbation 'vector'
$v_{\circ}^s, v_{\circ}^r$	local average phase velocities
Λ_L^S	2.5-D canonical relation
$\boldsymbol{\alpha}^s, \boldsymbol{\alpha}^r$	take-off directions at scattering point
$\boldsymbol{k}$	wave vector
$\boldsymbol{k}^s, \boldsymbol{k}^r$	wave vector for source and receiver rays, respectively
Λ_L^{CA}	common azimuth (CA) canonical relation
$\mathbf{L}^\star$	imaging operator
ψ	pseudodifferential cutoff
$\mathbf{N}$	normal operator
$\mathcal{N}$	kernel of normal operator
$\mathcal{J}$	extended Jacobian
$\boldsymbol{\nu}^m$	migration dip covector
μ_{LS}	scaled extended Jacobian
θ	scattering angle
Γ	matrix used in inversion
δ_{BL}	band-limited delta function
$\mathbf{K}$	angle transform
$\mathcal{K}_{mn}$	kernel of angle transform
Φ	phase function
$\underline{\boldsymbol{m}} = \{\boldsymbol{m}_1, \ldots\}$	collection of parameterized slices of background medium
J	misfit functional
Ξ	matrix used in reflection tomography by differential semblance
$\mathbf{c}^{(0)}$	background medium parameters
λ	statistical regularization parameter

Superscripts s and r indicate source and receiver respectively.

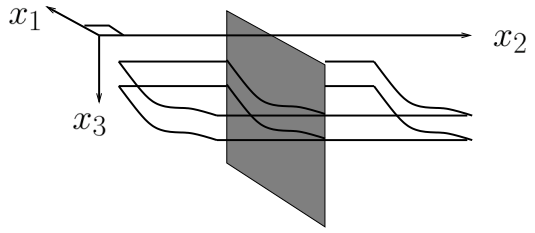

Figure 1. Cylindrical reflectors and the plane of consideration; (x_1, x_3)-plane.

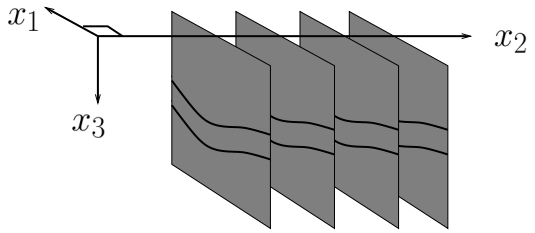

Figure 2. Parallell slices of the medium in the direction of the most dominant change.

1 INTRODUCTION

In this paper we derive general single scattering 2.5-D modelling and imaging-inversion formulas in anisotropic elastic media under precise assumptions. The lowest possible symmetry of the medium in this approach, in principle, is monoclinic, while the medium must be translationally invariant in the direction normal to the associated symmetry plane. All results are put in the context of common azimuth (CA) migration as discussed, for example, by de Hoop *et al* (2002). If the Earth varies in mostly two directions, a representative plane containing these directions will suffice in describing the subsurface; the 2.5-D framework applies approximately (it is exact if there are only two directions of change). This enables a fast computational way, through a slicewise approach, to reflection tomography. Further, it simplifies the ability to monitor the regularization of this kind of tomography. Figure 1 shows a representative slice in the direction of the dominant change while Figure 2 shows several parallel such slices in a medium with a smooth out-of-plane behavior.

Goldin (1986) and Červený (1981) considered the notion of 3-D wave propagation in 2-D media, the 2-D medium being contained in the mentioned plane. Bleistein (1986) introduced the notion of 2.5-D in seismic applications when restricting the attention to waves that travel and scatter in this plane alone consistent with the CA acquisition geometry if such geometry is aligned with the plane, but exhibit 3-D geometrical spreading. He considered the acoustic wave equation and derived modelling and Kirchoff migration formulas for this case. Several authors have since considered 2.5-D Kirchhoff migration in isotropic elastic media (Tygel *et al.* 1998; Dellinger *et al* 2000). Geoltrain (1989) extended the approach to Kirchhoff

migration in transversely isotropic media with a vertical symmetry axis.

The imaging-inversion results in this paper are derived using the inverse generalized Radon transform (GRT) (Miller, Oristaglio and Beylkin 1987) and using natural coordinates at each subsurface point to be imaged, namely scattering angle and migration dip. Sollid and Ursin (2003) derived a 2.5-D migration formula, using the GRT, in transversely isotropic media. A review of 2-D and 2.5-D inversion and migration is found in (Foss and Ursin 2003). Using the aforementioned choice of coordinates removes the use of a Beylkin determinant (de Hoop, Spencer and Burridge 1999). Additionally, this choice unravels caustics that may occur in an inhomogeneous medium giving rise to multivalued travel time functions. In the presence of caustics, strictly speaking, the GRT should be developed with Maslov Green's functions. However, de Hoop and Brandsberg-Dahl (2000) carried out an analysis that showed that as long as there are no caustics occurring at the source or receiver positions, through a stationary phase argument, the Maslov formulation reduces to a GRT based upon the geometrical ray approximation (GRA) for the Green's functions. Following this observation, we employ the GRA Green's function in our development. The formulas derived in this paper are applicable in the presence of multipathing and caustics under assumptions that will be clarified.

The high frequency linearized inversion, given a smooth background medium, yields the most singular part of the unknown medium contrast and is developed in the framework of pseudodifferential and Fourier integral operators (FIOs), see e.g. Duistermaat (1996). This was done in the acoustic case by Rakesh (1988), Hansen (1991) and in the anisotropic elastic.

In the presence of caustics, in the CA geometry, imaging artifacts may occur; for the acoustic case, see Nolan and Symes (1997). An artifact is defined as a false event in the image that is not contained in the medium contrast, i.e. an image reflector that is not there. The inversion is artifact-free under the so-called *Bolker condition* (Guillemin 1985). When this condition is violated, the image resulting from the inversion procedure will contain artifacts we have coined *artifacts of type 1*. The transformation of seismic data into common-image point gathers, based upon the GRT, can be viewed as introducing a restriction to a fixed scattering angle in the inversion formula (Brandsberg-Dahl *et al*. 2003b). This restriction in the presence of caustics will give rise to *artifacts of type 2* (for an exhaustive analysis of these artifacts, see Stolk (2002)). Brandsberg-Dahl *et al* (2003b) suppressed such artifacts by a procedure called focusing in dip by selecting contributions to the imaging-inversion integral from isochrones by an isochrone filter.

The outline of the paper is as follows. In section 2, we introduce the notation and the fundamental assumptions pertaining to 2.5-D. We also show by an example that, due to the anisotropy, an additional assumption is required to restrict the rays to travel in-plane, compared to Bleistein (1986). A detailed description of all aspects of the 2.5-D Born single scattering modelling formula is given. The derivation of this formula can be found in the Appendix A; it is based on approximating the out-of-plane integral of the 3-D Born modelling formula by the method of stationary phase (Bleistein 1986) given that there are no out-of-plane caustics. We give a description of which elastic parameters can be determined in the 2.5-D framework of CA data. A more detailed description of the parametrization and resolution of the smooth and perturbed parts of the medium in this context is given by Foss and Ursin (2003). Additionally, we give the precise assumptions subject to which our 2.5-D modelling is well defined and show how it pertains to the CA acquisition geometry. Section 3 contains the detailed guide through our inversion procedure, which is an analogue to least squares inversion. The inversion follows closely that of de Hoop and Brandsberg-Dahl (2000). We show that the 2-D Bolker condition pertaining to the symmetry plane implies the likewise condition in 3-D subject to the restriction to CA. First, we construct the adjoint (imaging) operator of the 2.5-D modelling operator. Second, we evaluate the normal operator and identify its 'inverse' up to leading order. Third, we compose this 'inverse' with mentioned adjoint to find the 2.5-D inversion operator. (For 'inverse', one should read parametrix, which is the inverse modulo smoothing operators.) The actual inversion result, for the most singular part of the medium contrast, is given in subsection 3.2 as an inverse by GRT in natural coordinates. In section 4 we present the 2.5-D transformation of the data to common-image point gathers. Section 5 shows results using the formulas derived in this paper applied to real ocean bottom cable (OBC) seismic data from the North Sea. We conclude with a discussion on future applications.

2 MODELLING

2.1 Green's functions in a smoothly varying medium

The geometrical ray approximation (GRA) to the Green's functions is a causal, short period approximate solution to the elastic wave equation, in the frequency domain given by

$$\rho(\boldsymbol{x})\omega^2 G_{in} + \partial_j(c_{ijkl}(\boldsymbol{x})\partial_l G_{kn}) = -\delta_{in}\delta(\boldsymbol{x}-\boldsymbol{x}^s) \qquad i,j,k,l,n = 1,2,3, \quad (1)$$

where ω is angular frequency and the position vector is denoted by $\boldsymbol{x} = (x_1, x_2, x_3)$, $\rho(\boldsymbol{x})$ and $c_{ijkl}(\boldsymbol{x})$ are density and the stiffness tensor, respectively. The Kronecker delta, δ_{in}, gives the source term on the right-hand side in the canonical directions, operative at the source point, $\boldsymbol{x}^s$, through the delta function δ. The summation convention applies here and in the following. The Green's function is a sum over the different wave modes, where each term is of the form

$$G_{ip}(\boldsymbol{x},\omega,\boldsymbol{x}^s) = A(\boldsymbol{x},\boldsymbol{x}^s)h_i^s(\boldsymbol{x})h_p(\boldsymbol{x}^s)e^{\mathrm{i}\omega T(\boldsymbol{x},\boldsymbol{x}^s)}, \quad (2)$$

in which $T(\boldsymbol{x},\boldsymbol{x}^s)$ is the travel time along the ray connecting $\boldsymbol{x}$ with $\boldsymbol{x}^s$. (We do not explicitly indicate the mode of propagation; we treat the modes of propagation separately.) h_i^s and h_p are components of the unit polarization vectors at the endpoints of the ray, where the superscript s indicates that this polarization vector is associated with the ray originating at $\boldsymbol{x}^s$.

This convention will be used in the following: superscripts s and r indicate the association of a variable with either a source or a receiver point, $\boldsymbol{x}^s$ and $\boldsymbol{x}^r$, respectively. $A(\boldsymbol{x},\boldsymbol{x}^s)$ is the amplitude, which becomes complex in the presence of caustics, and can be written in the form (Červený 2001)

$$A(\boldsymbol{x},\boldsymbol{x}^s) = \frac{e^{-\mathrm{i}\frac{\pi}{2}\kappa(\boldsymbol{x},\boldsymbol{x}^s)}}{4\pi[\rho(\boldsymbol{x})v^s(\boldsymbol{x})\rho(\boldsymbol{x}^s)v(\boldsymbol{x}^s)]^{1/2}|\det\,\mathbf{Q}_2(\boldsymbol{x},\boldsymbol{x}^s)|^{1/2}}. \quad (3)$$

Here, v^s and v are the phase velocities at $\boldsymbol{x}$ and $\boldsymbol{x}^s$, respectively, in the direction of the ray connecting these points. $|\det\,\mathbf{Q}_2(\boldsymbol{x},\boldsymbol{x}^s)|^{1/2}$ is the relative geometrical spreading factor given by

$$[Q_2]^{-1}_{ij}(\boldsymbol{x},\boldsymbol{x}^s) = -\frac{\partial^2 T(\boldsymbol{x},\boldsymbol{x}^s)}{\partial q_i^s \partial q_j}, \quad i,j=1,2, \quad (4)$$

where q_j and q_i^s are local surface coordinates on the wave front at the points $\boldsymbol{x}$ and $\boldsymbol{x}^s$, respectively. $\kappa(\boldsymbol{x},\boldsymbol{x}^s)$ is the KMAH index and counts the caustics that the ray encounters between $\boldsymbol{x}^s$ and $\boldsymbol{x}$; it accounts for the phase shifts this causes. The subtleties concerning the computation of this index in the presence of anisotropy for the quasi shear waves are elucidated in (Klimeš 1997).

We are concerned with 2.5-D modelling, and imaging-inversion of elastic waves in anisotropic media in the Born approximation. To justify the 2.5-D approach we need to invoke appropriate assumptions. Two of the assumptions pertains to restricting the ray geometry to the (x_1,x_3)-plane in the modelling, the first being:

Assumption 1. (Symmetries)
a) The medium is invariant in the out-of-plane direction (x_2).
b) The (x_1,x_3)-plane of propagation is a plane of mirror symmetry.

The translational invariance of assumption 1 a) guarantees that the out-of-plane wave slowness is constant. Assumption 1 b) ensures that the wave front is symmetric about the symmetry plane. The lowest possible anisotropic symmetry is then monoclinic which has only one plane of mirror symmetry.

Due to the symmetry we may choose one of the wave front coordinates to coincide with the out-of-plane direction, say $q_2 = x_2$. The first wave front coordinate, say q_1, is chosen in-plane. Thus, in the 2.5-D approach (due to assumption 1 b)), $\frac{\partial T(\boldsymbol{x},\boldsymbol{x}^s)}{\partial q_1^s}$ and $\frac{\partial^2 T(\boldsymbol{x},\boldsymbol{x}^s)}{\partial q_1}$ are equal functions in x_2 and hence $\frac{\partial^2 T(\boldsymbol{x},\boldsymbol{x}^s)}{\partial q_1^s \partial x_2} = \frac{\partial^2 T(\boldsymbol{x},\boldsymbol{x}^s)}{\partial x_2^s \partial q_1} = 0$. In those wave front coordinates, the relative geometrical spreading matrix in equation (5) becomes a diagonal matrix,

$$\mathbf{Q}_2(\boldsymbol{x},\boldsymbol{x}^s) = -\begin{bmatrix} \dfrac{1}{\dfrac{\partial^2 T(\boldsymbol{x},\boldsymbol{x}^s)}{\partial q_1^s \partial q_1}} & 0 \\ 0 & \dfrac{1}{\dfrac{\partial p_2}{\partial x_2}} \end{bmatrix} = \begin{bmatrix} Q_2^{||}(\boldsymbol{x},\boldsymbol{x}^s) & 0 \\ 0 & Q_2^{\perp}(\boldsymbol{x},\boldsymbol{x}^s) \end{bmatrix}, \quad (5)$$

where $Q_2^{||}(\boldsymbol{x},\boldsymbol{x}^s)$ and $Q_2^{\perp}(\boldsymbol{x},\boldsymbol{x}^s)$ are the in-plane and out-of-plane relative geometrical spreading factors, respectively. This structure implies that the relative geometrical spreading in equation (3) factors into an in-plane and an out-of-plane component,

$$|\det\,\mathbf{Q}_2(\boldsymbol{x},\boldsymbol{x}^s)|^{1/2} = |Q_2^{||}(\boldsymbol{x},\boldsymbol{x}^s)Q_2^{\perp}(\boldsymbol{x},\boldsymbol{x}^s)|^{1/2}. \quad (6)$$

Note that the argument in equation (5) for the splitting of the in-plane and out-of-plane spreading is not dependent on the actual constant value of p_2.

2.2 Scattering in the Born approximation

The 2.5-D Born modelling formula is derived from the 3-D Born modelling formula by a stationary phase argument integrating out the out-of-plane coordinate, following Bleistein (1986). The domain in the symmetry plane in which the 2-D scattering takes place is denoted by $X \subset \mathbb{R}^2$. From now on, let $\boldsymbol{x} = (x_1,x_3) \in X$.

The stationary phase argument involves the stationarity condition (Appendix, equation (A3))

$$\partial_{x_2}(T(\boldsymbol{x}^s,\boldsymbol{x}) + T(\boldsymbol{x},\boldsymbol{x}^r)) = p_2^s + p_2^r = 0, \quad (7)$$

where $\boldsymbol{p}^2 = (p_1^s,p_2^s,p_3^s)$ and $\boldsymbol{p}^r = (p_1^r,p_2^r,p_3^r)$ are the slowness vectors associated with the source ray and the receiver ray, respectively. We wish to restrict our attention to rays that only travel in-plane. However, the stationary phase argument in equation (7) admits out-of-plane contributions. A simple example that satisfies equation (7), using p_2^s equal a constant, for qSV-qSV scattering ('q' stands for 'quasi' in the following) is illustrated in Figure 4. The medium is transversely isotropic with a vertical symmetry axis (x_3-axis). By controlling the Thomsen parameters, ϵ and δ (Thomsen 1986), we may change the shape of the slowness surface

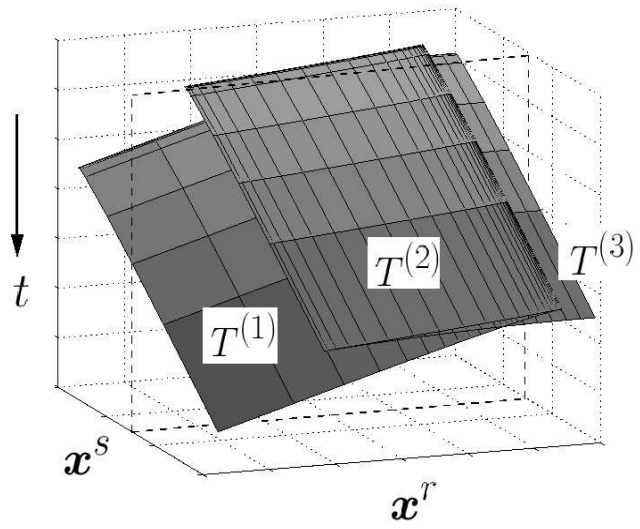

Figure 3. Triplication of the recorded wave field with travel time functions per branch denoted $T^{(1)}$, $T^{(2)}$ and $T^{(3)}$. Dotted plane indicates a common shot gather.

smoothly as shown on the right of the figure for three different depths in the model used in the ray tracing on the left. All axes are given in meters. The group velocity vector, $\mathbf{V}$, is perpendicular to the slowness surface and governs the direction of the ray. This is indicated with the surface normal to the slowness surface, $\hat{n}$. As suggested in the figure, we may change smoothly the direction of the energy velocity, sending the rays out of the plane and back again while keeping p_2 fixed (implication of assumption 1 a)). Two rays are shot at a small positive and negative angle with the x_3-axis in the out-of-plane direction ($p_1^s = p_1^r = 0$) from $(x_1, x_2, x_3) = (0, 0, 200)$. They travel in the (x_2, x_3)-plane and intersect at the point $(0, 0, 2800)$ with incoming angles following Snell's law and satisfying equation (7). We note that the anisotropy in this example allows triplications on the symmetry axis, which is unusual in a sedimentary sequence setting.

We admit in-plane scattering events only, by imposing:

Assumption 2. (Seismic phase restriction) *Only seismic events with at least one ray, or leg, associated with a wave type that pertains to a convex slowness surface are considered.*

If one of the ray legs is associated with a convex slowness surface, the only solution to equation (7) is $p_2^r = p_2^s = 0$. Due to the symmetry in assumption 1 b) this also means that $V_2^s = V_2^r = 0$. This follows because $p_2^r = -p_2^s \neq 0$ on a convex slowness surface will induce group velocity vectors pointing out of the plane (the middle slowness surface on the right of Figure 4 illustrates this). The group vectors send seismic energy away from the plane never to return. In particular, P waves always have a convex slowness surface (Musgrave 1970); hence, qP-qP and qP-qSV scattering events always satisfy assumption 2.

The medium parameters are represented by a sum of a smooth part, $\rho^{(0)}$ and $c_{ijkl}^{(0)}$, and a singular perturbation, $\rho^{(1)}$ and $c_{ijkl}^{(1)}$:

$$\rho(\boldsymbol{x}) = \rho^{(0)}(\boldsymbol{x}) + \rho^{(1)}(\boldsymbol{x}), \quad c_{ijkl}(\boldsymbol{x}) = c_{ijkl}^{(0)}(\boldsymbol{x}) + c_{ijkl}^{(1)}(\boldsymbol{x}). \tag{8}$$

Note that both the smooth part and the perturbation are restricted in accordance with assumption 1a) and b) making the reflectors parts of the cylindrical surfaces (see Figure 1). In the Born approximation, the waves travel in the smooth part of the medium and are scattered off the perturbation once. In the imaging-inversion problem the smooth medium is assumed to be known. It is the medium perturbation we will invert for. The multicomponent data collected in a seismic experiment, u_{mn}, under the condition of a smooth background, will be, in this approximation, the asymptotic part of the modelling formula. The subscripts indicate that u_{mn} is the m-component of the recorded wave field due to a body force in the n-direction. The data (scattered wave field) can be modelled by an operator $\mathbf{L}$ acting on the medium perturbation (see Appendix A for a detailed derivation, where U_{mn} is the time-Fourier transform of the data u_{mn})

$$\begin{aligned} u_{mn}(\boldsymbol{x}^s, \boldsymbol{x}^r, t) &= \mathbf{L}\mathbf{c}^{(1)}(\boldsymbol{x}^s, \boldsymbol{x}^r, t) \\ &\approx \sum_{i \in I} \sqrt{\frac{\mathrm{i}}{2\pi}} \int_X \int_{\mathbb{R}} h_m(\boldsymbol{x}^r) \omega^{3/2} \rho^{(0)}(\boldsymbol{x}) \frac{A^{||}(\boldsymbol{x}^s, \boldsymbol{x}) A^{||}(\boldsymbol{x}, \boldsymbol{x}^r)}{\mathcal{L}^{\perp}(\boldsymbol{x}^r, \boldsymbol{x}, \boldsymbol{x}^s)} \\ &\quad \cdot \mathbf{w}^T(\boldsymbol{x}^r, \boldsymbol{x}, \boldsymbol{x}^s) \mathbf{c}^{(1)}(\boldsymbol{x}) e^{\mathrm{i}\omega(T^{(i)}(\boldsymbol{x}^r, \boldsymbol{x}, \boldsymbol{x}^s) - t)} h_n(\boldsymbol{x}^s) \mathrm{d}\omega \mathrm{d}\boldsymbol{x}. \end{aligned} \tag{9}$$

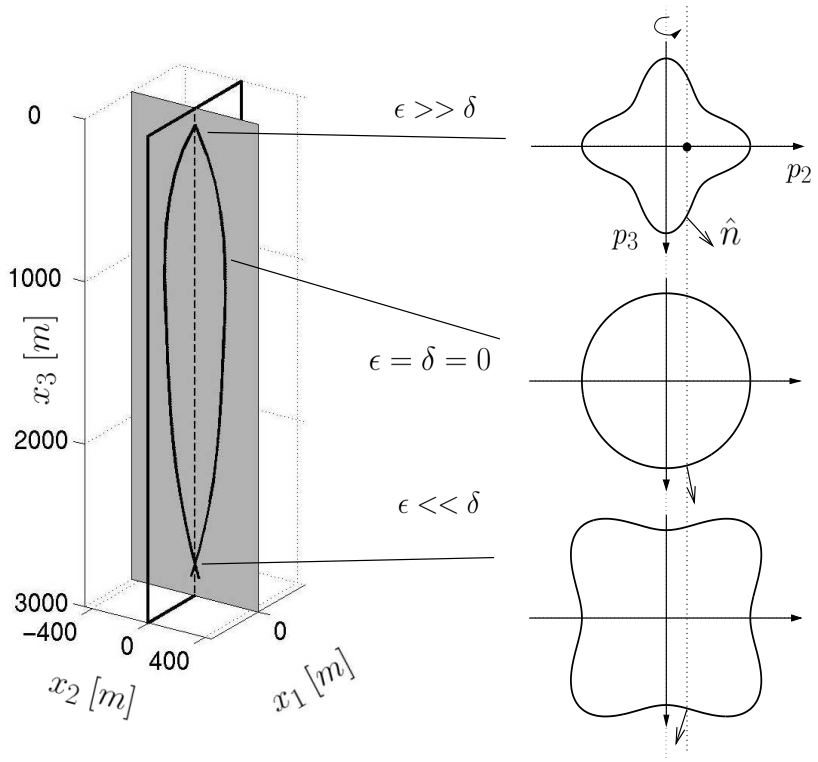

Figure 4. Example of rays travelling out-of-plane that are in the stationary point set equation (7)

Here, $T^{(i)}$ is the two-way travel time given by

$$T^{(i)}(\boldsymbol{x}^r, \boldsymbol{x}, \boldsymbol{x}^s) = T(\boldsymbol{x}^s, \boldsymbol{x}) + T(\boldsymbol{x}, \boldsymbol{x}^r). \tag{10}$$

(Note that the modelling equation is valid up to leading order since we inserted the GRA amplitudes in the oscillatory integral representations for the Green's functions.) We consider $\boldsymbol{x}^s, \boldsymbol{x}^r \in X$. Restricting $\boldsymbol{x}^s, \boldsymbol{x}^r$ further to smooth source and receiver lines forming the manifold $\Sigma \subset \partial X \times \partial X$, we introduce the 2-D acquisition manifold $Y = \Sigma \times \mathbb{R}_{\geq 0} \ni (\boldsymbol{x}^s, \boldsymbol{x}^r, t)$, where t is time. The signifi cance of the superscript (i) on $T^{(i)}$ is in the case of multivaluedness of two-way travel time in the presence of caustics. In that case $i \in I$ labels the branches of the two-way travel time and I is the collection of them. The set $\{T^{(i)}\}_{i\in I}$ describes the two-way travel times for all branches. Each $T^{(i)}$ is defi ned on a subset $D^{(i)}$ of $\Sigma \times X$, i.e. a particular subset of acquisition and scattering points $(\boldsymbol{x}^s, \boldsymbol{x}^r, \boldsymbol{x})$. In a generic inhomogeneous medium, caustics will form. Figure 3 shows an example of multivaluedness: a triplication in the recorded wave fi eld, the dotted plane indicating how this is recorded for a single source. The branches are assigned a number to separate them indicated on the travel time functions $T^{(1)}$, $T^{(2)}$, $T^{(3)}$. We will omit this indexing of the branches for clarity of notation until the distinction becomes important again (see the discussion on artifacts). The sum over the different travel time branches in equation (9) will thus be suppressed and assumed implicit in the following.

The amplitudes, $A^{||}(\boldsymbol{x}^s, \boldsymbol{x})$ and $A^{||}(\boldsymbol{x}, \boldsymbol{x}^r)$, are the GRA amplitudes (see equation (5)) with only the in-plane geometrical spreading factor $Q_2^{||}$, for example

$$A^{||}(\boldsymbol{x}, \boldsymbol{x}^s) = \frac{e^{-\mathrm{i}\frac{\pi}{2}\kappa(\boldsymbol{x}\ ,\boldsymbol{x}^{\ s})\mathrm{sgn}\,\omega}}{4\pi[\rho(\boldsymbol{x})v^s(\boldsymbol{x})\rho(\boldsymbol{x}^s)v(\boldsymbol{x}^s)]^{1/2}|Q_2^{||}(\boldsymbol{x}, \boldsymbol{x}^s)|^{1/2}}. \tag{11}$$

The two-way out-of-plane geometrical spreading is given by

$$\mathcal{L}^{\perp}(\boldsymbol{x}^r, \boldsymbol{x}, \boldsymbol{x}^s) = |Q_2^{\perp}(\boldsymbol{x}^s, \boldsymbol{x}) + Q_2^{\perp}(\boldsymbol{x}, \boldsymbol{x}^r)|^{1/2}. \tag{12}$$

The out-of-plane geometrical spreading $Q_2^{\perp}$ for the source ray, for example, can be expressed as

$$Q_2^{\perp}(\boldsymbol{x}^s, \boldsymbol{x}) = \int_{ray} \frac{V_2}{p_2}\mathrm{d}t, \tag{13}$$

where the integral is along the ray parametrized by travel time t connecting $\boldsymbol{x}^s$ with $\boldsymbol{x}$. The integrand V_2/p_2 tends to a value as

both V_2, p_2 tend to zero (in accordance with the 2.5-D approach, where $p_2 = 0, V_2 = 0$). Closed form expressions for the integrand for isotropic, transversely isotropic and orthorhombic media can be found in Ettrich *et al.* (2002), equations (15), (19) and (22), respectively. The medium perturbations are collected in the matrix $\mathbf{c}^{(1)}(\boldsymbol{x})$ and the radiation patterns equivalently in $\mathbf{w}(\boldsymbol{x}^r, \boldsymbol{x}, \boldsymbol{x}^s)$. They will be defi ned in the next subsection.

Remark 1. *We restrict our analysis to the part of phase space where out-of-plane caustics do not occur. Thus we mute events associated with rays forming out-of-plane caustics (see Remark 4 in the appendix).*

2.2.1 Medium perturbations and radiation patterns

Since by assumption 1, the medium is restricted to monoclinic or higher symmetry, there are at most 13 stiffness parameters plus density as independent unknown distributions. The stiffness tensor is given by (if the (x_1, x_3)-plane is the symmetry plane):

$$[c_{ijkl}] = \begin{bmatrix} c_{1111} & c_{1122} & c_{1133} & 0 & c_{1113} & 0 \\ c_{1122} & c_{2222} & c_{2233} & 0 & c_{2213} & 0 \\ c_{1133} & c_{2233} & c_{3333} & 0 & c_{3313} & 0 \\ 0 & 0 & 0 & c_{2323} & 0 & c_{2312} \\ c_{1113} & c_{2213} & c_{3313} & 0 & c_{1313} & 0 \\ 0 & 0 & 0 & c_{1223} & 0 & c_{1212} \end{bmatrix}. \tag{14}$$

The medium perturbations are collected in the 14×1 matrix for monoclinic anisotropy (Burridge *et al.* 1998)

$$\mathbf{c}^{(1)}(\boldsymbol{x}) = \left\{ \frac{\rho^{(1)}(\boldsymbol{x})}{\rho^{(0)}(\boldsymbol{x})}, \frac{c^{(1)}_{ijkl}(\boldsymbol{x})}{\rho^{(0)}(\boldsymbol{x}) v^s_\circ(\boldsymbol{x}) v^r_\circ(\boldsymbol{x})} \right\}, \tag{15}$$

where $v^s_\circ$ and $v^r_\circ$ are local phase velocities averaged over all phase angles. These are introduced for computational purposes so that the matrix has components of similar magnitude (Burridge *et al.* 1998). We restrict the indices of $c^{(1)}_{ijkl}$ to the 13 independent components of the stiffness tensor (cf. (12)). With higher symmetry, such as isotropy, the matrix reduces accordingly (Beylkin and Burridge 1990). The radiation pattern matrix is defi ned similarly as the 14×1 matrix (Burridge *et al.* 1998)

$$\mathbf{w}(\boldsymbol{x}^r, \boldsymbol{x}, \boldsymbol{x}^s) = \left\{ h^s_m(\boldsymbol{x}) h^r_m(\boldsymbol{x}), [h^s_i(\boldsymbol{x}) p^s_j(\boldsymbol{x}) h^r_k(\boldsymbol{x}) p^r_l(\boldsymbol{x})] v^s_\circ(\boldsymbol{x}) v^r_\circ(\boldsymbol{x}) \right\}, \tag{16}$$

where the indices follow those of the stiffness matrix in the ordering defi ned by the matrix or inner product $\mathbf{w}^T(\boldsymbol{x}^r, \boldsymbol{x}, \boldsymbol{x}^s)\mathbf{c}^{(1)}(\boldsymbol{x})$ in the modelling equation (9). Since the out-of-plane slowness will be zero, $p^s_2 = p^r_2 = 0$, we see from equation (16) that the contribution vanishes if $j, l = 2$ in $c^{(1)}_{ijkl}$. In view of assumptions 1 and 2, having $p^s_2 = p^r_2 = 0$, the polarizations of qP and qSV waves satisfy $h_2 = 0$. Thus the parameters we can invert for from qP-qP and qP-qSV scattering are the 7 parameters out of the 14 independent ones in a monoclinic medium, $c^{(1)}_{1111}, c^{(1)}_{1133}, c^{(1)}_{3333}, c^{(1)}_{1113}, c^{(1)}_{3313}, c^{(1)}_{1313}$ and density $\rho^{(1)}$ ($h_2 = 0$, and hence the contributions for $i, k = 2$ in $c^{(1)}_{ijkl}$ are zero). The kinematic aspects for a monoclinic background medium are governed by the same partitioning of parameters (Chapman and Pratt 1992; Foss and Ursin 2003).

Remark 2. *In imaging, the smooth background medium is given, and hence the relevant amplitudes can be computed in the lowest possible symmetry admitted by the 2.5-D framework: monoclinic. However, for inversion and reflection tomography, having observations restricted to the plane under consideration, only parameters associated with this plane can be estimated. Hence the lowest possible symmetry is transversely isotropic with a symmetry axis in the plane. Due to the rotational symmetry of the medium, parameters needed in out-of-plane amplitude calculations are found from in-plane propagation (Ettrich et al 2002; equation (19)).*

2.3 The modelling operator in common azimuth

The 3-D Born modelling operator has been shown to be a Fourier integral operator (FIO) under the mild conditions that there are no direct rays between the source and the receiver reaching the medium perturbation (i.e. rays that have scattered off a subsurface point over an angle π) and no grazing rays (i.e. rays that reach the acquisition surface tangentially to the surface) (Rakesh 1988; Hansen 1991). The 3-D modelling operator with common azimuth (CA) acquisition geometry (Biondi and Palacharla 1996) is also an FIO under similar conditions (Nolan and Symes 1997; de Hoop *et al* 2003). 2.5-D implies CA (but not the other way) aligning our symmetry plane with the acquisition geometry, i.e. $x^s_2 = x^r_2$. We conclude that the 2.5-D modelling operator (9) has the properties of a FIO, and has the following canonical relation (superscript S indicates that this is a canonical relation in two space dimensions coinciding with the symmetry plane)

$$\Lambda^S_L = \{(\boldsymbol{x}^s(\boldsymbol{x}, \boldsymbol{\alpha}^s), \boldsymbol{x}^r(\boldsymbol{x}, \boldsymbol{\alpha}^r), T(\boldsymbol{x}^s(\boldsymbol{x}, \boldsymbol{\alpha}^s), \boldsymbol{x}, \boldsymbol{x}^r(\boldsymbol{x}, \boldsymbol{\alpha}^r)), \boldsymbol{k}^s(\boldsymbol{x}, \boldsymbol{\alpha}^s, \omega), \boldsymbol{k}^r(\boldsymbol{x}, \boldsymbol{\alpha}^r, \omega), \omega; \\ \boldsymbol{x}, -\boldsymbol{k}(\boldsymbol{x}^s(\boldsymbol{x}, \boldsymbol{\alpha}^s), \boldsymbol{x}, \boldsymbol{x}^r(\boldsymbol{x}, \boldsymbol{\alpha}^r), \omega)) | (\boldsymbol{x}, \boldsymbol{\alpha}^s, \boldsymbol{\alpha}^r) \in K, \omega \in \mathbb{R} \setminus 0\}. \tag{17}$$

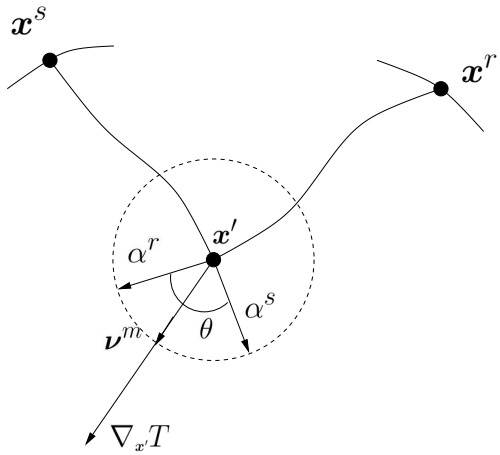

Figure 5. Coordinate systems.

The canonical relation is a table that describes how reflectors induce reflections geometrically. The canonical relation is intimately connected to ray tracing in phase space (Billette and Lambaré 1998). $\boldsymbol{\alpha}^s(\boldsymbol{x})$ and $\boldsymbol{\alpha}^r(\boldsymbol{x})$ are the take-off directions of the rays originating at the scattering point $\boldsymbol{x} \in X$ and are given by the unit phase vectors $\boldsymbol{\alpha}^s(\boldsymbol{x}) = \boldsymbol{p}^s(\boldsymbol{x})/|\boldsymbol{p}^s(\boldsymbol{x})|$ and $\boldsymbol{\alpha}^r(\boldsymbol{x}) = \boldsymbol{p}^r(\boldsymbol{x})/|\boldsymbol{p}^r(\boldsymbol{x})|$ (see Figure 5). K is an appropriately chosen subset of $X \times S^1 \times S^1$ (S^1 is the unit circle). On the canonical relation (17) $\boldsymbol{k}(\boldsymbol{x}^s(\boldsymbol{x},\boldsymbol{\alpha}^s),\boldsymbol{x},\boldsymbol{x}^r(\boldsymbol{x},\boldsymbol{\alpha}^r),\omega) = \omega\nabla_{\boldsymbol{x}}\,T(\boldsymbol{x}^s(\boldsymbol{x},\boldsymbol{\alpha}^s),\boldsymbol{x},\boldsymbol{x}^r(\boldsymbol{x},\boldsymbol{\alpha}^r))$ has the interpretation of wave vector (the Fourier dual of $\boldsymbol{x}$). Given a take-off direction ($\boldsymbol{\alpha}^s$ or $\boldsymbol{\alpha}^r$) at a scattering point $\boldsymbol{x}$, rays are traced to an acquisition line giving unique intersection points ($\boldsymbol{x}^s = \boldsymbol{x}^s(\boldsymbol{x},\boldsymbol{\alpha}^s)$ or $\boldsymbol{x}^r = \boldsymbol{x}^r(\boldsymbol{x},\boldsymbol{\alpha}^r)$) as well as slowness vectors; these slowness vectors are projected onto the aforementioned acquisition line resulting into $\boldsymbol{k}^s/\omega$, $\boldsymbol{k}^r/\omega$, from which $\boldsymbol{k}^s(\boldsymbol{x},\boldsymbol{\alpha}^s,\omega)$, $\boldsymbol{k}^r(\boldsymbol{x},\boldsymbol{\alpha}^r,\omega)$ are derived.

Remark 3. *The 3-D CA Born scattering operator yields the following canonical relation (compare with the 2.5-D Born modelling operator above in equation (17))*

$$\Lambda_L^{CA} = \{(x_1^s, x_2^s, x_1^r, t, k_1^s, k_2^s + k_2^r, k_1^r, \omega; x_1, x_2, x_3, -k_1, -k_2, -k_3)\}\,, \tag{18}$$

where $(x_1^s, x_2^s, x_1^r, x_2^s, t, k_1^s, k_2^s, k_1^r, k_2^r, \omega; x_1, x_2, x_3, -k_1, -k_2, -k_3)$ are contained in the Born modelling 3-D canonical relation Λ_L^{3D} which is the counterpart of Λ_L^S in three space dimensions (e.g. Stolk and de Hoop (2002)). Note that t is here a general two-way travel time function in order to separate it from the one in equation (10) which is limited to a plane. Due to the translational invariance of the medium, assumption 1a), the individual k_2^s and k_2^r are preserved. Hence at the scattering point $k_2 = k_2^s + k_2^r$, in which k_2^s and k_2^r attain their values at the source and the receiver, respectively. This equality can also be written as $k_2 = \omega(p_2^s + p_2^r)$. In view, again, of the invariance in the out-of-plane direction the 2-component of any reflector dips must vanish. Hence, given a source and a receiver ray such that $k_2^s + k_2^r \neq 0$, no specular reflection will return to the acquisition manifold. This is also confirmed by the stationary phase argument underlying the 2.5-D analysis, see equation (7).

The modelling operator maps the medium perturbation to the data

$$\mathbf{L} : \mathbf{c}^{(1)} \rightarrow u_{mn}\,. \tag{19}$$

3 2.5-D IMAGING – INVERSION

In this section, we develop the inversion for the medium parameters collected in the matrix $\mathbf{c}^{(1)}$ in equation (15). The inversion can be viewed as an analogue to matrix least-squares inversion. In this context, we introduce the adjoint, $\mathbf{L}^\star$, of the forward operator the so-called *imaging operator*, and apply it to equation (9),

$$\mathbf{L}^\star(\psi\mathbf{L}\mathbf{c}^{(1)}) = \mathbf{L}^\star u, \tag{20}$$

where u is shorthand for the data (indices are suppressed, see the discussion below). The composition of the imaging with the forward operator gives us the *normal operator*, $\mathbf{N} = \mathbf{L}^\star\psi\mathbf{L}$. The operator $\mathbf{L}^\star$ images reflectors properly if $\mathbf{L}^\star\psi\mathbf{L}$ is a pseudodifferential operator (Stolk and de Hoop 2002). Here ψ is a pseudodifferential cutoff ('tapered mute') to ensure that the mild conditions of subsection 2.3, making the modelling operator an FIO, are satisfied. In the following we will refer to $\mathbf{L}^\star\psi\mathbf{L}$ as the normal operator $\mathbf{N}$ where ψ is assumed implicitly.

Assumption 3. *The projection of the canonical relation Λ_L^S of the 2.5-D modelling operator on the acquisition variables $(\boldsymbol{x}^s, \boldsymbol{x}^r, t, \boldsymbol{k}^s, \boldsymbol{k}^r, \omega)$ is one-to-one.*

This assumption is consistent with a 2-D Bolker condition (Guillemin 1985), for the acoustic case see Ten Kroode *et al.* (1998). It means that $(\boldsymbol{x}^s, \boldsymbol{x}^r, t, \boldsymbol{k}^s, \boldsymbol{k}^r, \omega)$ determine a scattering point $\boldsymbol{x} \in X$ and associated wave vector $\boldsymbol{k}$, uniquely and smoothly. This condition ensures that the normal operator is an elliptic pseudodifferential operator. Hence the procedure of imaging the modelled data, equation (20), does not generate reflectors that were not there to begin with, i.e. that are not present in $\mathbf{c}^{(1)}$.

Since $\mathbf{N}$ is elliptic and pseudodifferential we can construct its parametrix, denoted by $\langle \mathbf{N}^{-1} \rangle$. The brackets indicate that this is a pseudo inverse. Following the analogue of least-squares inversion, an estimate of the medium perturbation in equation (15) can be recovered from the composition

$$\hat{\mathbf{c}}^{(1)} \approx \langle \mathbf{N}^{-1} \rangle \mathbf{L}^{\star} u, \tag{21}$$

where u is the data. If assumption 3 is violated we generate artifacts (discussed in the introduction). A less restrictive condition and a discussion of the implied artifacts can be found in de Hoop and Brandsberg-Dahl (2000) and Stolk (2000).

In view of Remark 3, assumption 3 (or the 2-D Bolker condition) in the symmetry plane implies the 3-D CA Bolker condition. This condition encompasses that for any point in Λ_L^{CA}, i.e., for an intersecting pair of source and receiver rays, given $(x_1^s, x_2^s, x_1^r, x_2^s, t, k_1^s, k_2^s + k_2^r, k_1^r, \omega)$, there is only one (t, k_2^s) that explains the reflection.

3.1 The adjoint scattering (imaging) and the normal operators

In this subsection, we evaluate the adjoint $\mathbf{L}^{\star}$ of the modelling operator $\mathbf{L}$ and deduce the leading order contribution to the normal operator $\mathbf{N}$ for which we can derive a parametrix. We will write the action of the normal operator as a pseudodifferential operator, i.e. as integrals over $\boldsymbol{x}$ and its Fourier dual $\boldsymbol{k}$, the wave vector. The inverse of the integrand thus obtained (the integrand yields the so-called *symbol* of the normal operator) generates the 'inverse' of the normal operator up to leading order.

We let the acquisition coordinates be defined on the two acquisition lines in the symmetry plane, ∂S and ∂R for sources and receivers, respectively. By the reciprocity theorem of the time-correlation type found in de Hoop and de Hoop (2000) the adjoint or imaging operator $\mathbf{L}^{\star}$ can be written

$$\begin{aligned}\mathbf{L}^{\star} u(\boldsymbol{x}') \approx \frac{1}{\sqrt{2\pi \mathrm{i}}} \int_{\partial S \times \partial R} \int_{\mathbb{R}} \int_{\mathbb{R}\geq 0} \omega'^{3/2} \rho^{(0)}(\boldsymbol{x}') \frac{(A^{||}(\boldsymbol{x}^s, \boldsymbol{x}') A^{||}(\boldsymbol{x}', \boldsymbol{x}^r))^{\star}}{\mathcal{L}^{\perp}(\boldsymbol{x}^r, \boldsymbol{x}', \boldsymbol{x}^s)^{\star}} \\ \cdot \mathbf{w}(\boldsymbol{x}^r, \boldsymbol{x}', \boldsymbol{x}^s) h_m(\boldsymbol{x}^r; \boldsymbol{x}') u_{mn}(\boldsymbol{x}^s, \boldsymbol{x}^r, t) h_n(\boldsymbol{x}^s; \boldsymbol{x}') e^{-\mathrm{i}\omega'(T(\boldsymbol{x}^r, \boldsymbol{x}', \boldsymbol{x}^s) - t)} \mathrm{d}t \mathrm{d}\omega' \mathrm{d}\boldsymbol{x}^s \mathrm{d}\boldsymbol{x}^r,\end{aligned} \tag{22}$$

where ω' is the frequency and * indicates the adjoint as well as complex conjugation. The polarization vectors associated with the scattering off the point $\boldsymbol{x}'$ are denoted by $h_m(\boldsymbol{x}^r; \boldsymbol{x}')$ and $h_n(\boldsymbol{x}^s; \boldsymbol{x}')$ to distinguish them from the polarization vectors due to the scattering off $\boldsymbol{x}$ as in equation (9). Note that there is a summation over the different indices of the data u_{mn} in the integrand of the adjoint, following the summation convention. Hence the notation of $\mathbf{L}^{\star}$ acting on all the data denoted by u. Note also that $\mathbf{w} = (\mathbf{w}^T)^{\star}$.

Composing the imaging operator with the modelling operator (having used a pseudodifferential cutoff for when it fails to satisfy assumption 3) gives us the normal operator. The u_{mn} from the modelling equation (9) is inserted into the above expression to yield

$$\begin{aligned}\mathbf{L}^{\star} \psi \mathbf{L} \mathbf{c}^{(1)}(\boldsymbol{x}') \approx \\ \frac{1}{2\pi} \int_{\partial S \times \partial R} \int_X \int_{\mathbb{R}} \int_{\mathbb{R}} \int_{\mathbb{R}\geq 0} \omega'^{3/2} \omega^{3/2} \rho^{(0)}(\boldsymbol{x}') \rho^{(0)}(\boldsymbol{x}) \frac{(A^{||}(\boldsymbol{x}^s, \boldsymbol{x}') A^{||}(\boldsymbol{x}', \boldsymbol{x}^r))^{\star}}{\mathcal{L}^{\perp}(\boldsymbol{x}^r, \boldsymbol{x}', \boldsymbol{x}^s)^{\star}} \frac{A^{||}(\boldsymbol{x}^s, \boldsymbol{x}) A^{||}(\boldsymbol{x}, \boldsymbol{x}^r)}{\mathcal{L}^{\perp}(\boldsymbol{x}^r, \boldsymbol{x}', \boldsymbol{x}^s)} \\ \cdot e^{\mathrm{i}\omega(T(\boldsymbol{x}^r, \boldsymbol{x}, \boldsymbol{x}^s) - t) - \mathrm{i}\omega'(T(\boldsymbol{x}^r, \boldsymbol{x}', \boldsymbol{x}^s) - t)} \mathrm{d}t \mathrm{d}\omega \mathrm{d}\omega' \mathrm{d}\boldsymbol{x} \mathrm{d}\boldsymbol{x}^s \mathrm{d}\boldsymbol{x}^r.\end{aligned} \tag{23}$$

If assumption 3 is satisfied it is indeed an elliptic pseudodifferential operator. The integral over t yields a delta function $\delta(\omega - \omega')$ so we can collapse the integral over ω' and set $\omega = \omega'$. Invoking a Taylor expansion about $\boldsymbol{x}'$ for the two-way travel time $T(\boldsymbol{x}^r, \boldsymbol{x}, \boldsymbol{x}^s)$ yields, due to the fact that higher order derivatives give smoother contributions to the amplitude (Hörmander 1985a) through expansion of the exponential,

$$\omega[T(\boldsymbol{x}^r, \boldsymbol{x}, \boldsymbol{x}^s) - T(\boldsymbol{x}^r, \boldsymbol{x}', \boldsymbol{x}^s)] = \omega[(\nabla_{\boldsymbol{x}'} T)(\boldsymbol{x}^r, \boldsymbol{x}', \boldsymbol{x}^s) \cdot (\boldsymbol{x} - \boldsymbol{x}')] + \ldots. \tag{24}$$

Inserting (24) in the phase function of the normal operator yields

$$\mathbf{Nc}^{(1)}(\boldsymbol{x}') \approx \int_{\partial S\times\partial R}\int_X\int_{\mathbb{R}} \omega^3\rho^{(0)}(\boldsymbol{x}')\rho^{(0)}(\boldsymbol{x})\frac{(A^{||}(\boldsymbol{x}^s,\boldsymbol{x}')A^{||}(\boldsymbol{x}',\boldsymbol{x}^r))^\star}{\mathcal{L}^\perp(\boldsymbol{x}^r,\boldsymbol{x}',\boldsymbol{x}^s)^\star}\frac{A^{||}(\boldsymbol{x}^s,\boldsymbol{x})A^{||}(\boldsymbol{x},\boldsymbol{x}^r)}{\mathcal{L}^\perp(\boldsymbol{x}^r,\boldsymbol{x}',\boldsymbol{x}^s)}$$
$$\cdot\,\mathbf{w}(\boldsymbol{x}^r,\boldsymbol{x}',\boldsymbol{x}^s)\mathbf{w}^T(\boldsymbol{x}^r,\boldsymbol{x},\boldsymbol{x}^s)\mathbf{c}^{(1)}(\boldsymbol{x})h_m(\boldsymbol{x}^r)h_m(\boldsymbol{x}^r;\boldsymbol{x}')h_n(\boldsymbol{x}^s)h_n(\boldsymbol{x}^s;\boldsymbol{x}')$$
$$\cdot\, e^{\mathrm{i}\omega\nabla_{\boldsymbol{x}'}T(\boldsymbol{x}^r,\boldsymbol{x}',\boldsymbol{x}^s)\cdot(\boldsymbol{x}-\boldsymbol{x}')}\mathrm{d}\omega\mathrm{d}\boldsymbol{x}\mathrm{d}\boldsymbol{x}^s\mathrm{d}\boldsymbol{x}^r. \quad (25)$$

The most dominant contribution to the oscillatory integral (25) occurs when $\boldsymbol{x}$ and $\boldsymbol{x}'$ are near one another making up a small neighbourhood of support (Beylkin 1985). Additionally, the amplitudes, polarization vectors and the radiation patterns vary slowly compared to any other part of the integrand. We may then assume that they are constant in a small neighbourhood of $\boldsymbol{x}'$. Since the polarization vectors are normalized we obtain

$$\mathbf{Nc}^{(1)}(\boldsymbol{x}') \approx \int_{\partial S\times\partial R}\int_X\int_{\mathbb{R}} \omega^3\rho^{(0)}(\boldsymbol{x}')^2\frac{|A^{||}(\boldsymbol{x}^s,\boldsymbol{x}')A^{||}(\boldsymbol{x}',\boldsymbol{x}^r))|^2}{|\mathcal{L}^\perp(\boldsymbol{x}^r,\boldsymbol{x}',\boldsymbol{x}^s)|^2}$$
$$\cdot\,\mathbf{w}(\boldsymbol{x}^r,\boldsymbol{x}',\boldsymbol{x}^s)\mathbf{w}^T(\boldsymbol{x}^r,\boldsymbol{x}',\boldsymbol{x}^s)\mathbf{c}^{(1)}(\boldsymbol{x})e^{\mathrm{i}\omega\nabla_{\boldsymbol{x}'}T(\boldsymbol{x}^r,\boldsymbol{x}',\boldsymbol{x}^s)\cdot(\boldsymbol{x}-\boldsymbol{x}')}\mathrm{d}\omega\mathrm{d}\boldsymbol{x}\mathrm{d}\boldsymbol{x}^s\mathrm{d}\boldsymbol{x}^r. \quad (26)$$

3.1.1 Subsurface coordinates

We choose to work with coordinates directly at the imaging point $\boldsymbol{x}'$ and introduce the change of variables

$$(\boldsymbol{x}',\boldsymbol{x}^s,\boldsymbol{x}^r) \leftarrow (\boldsymbol{x}',\boldsymbol{\alpha}^s,\boldsymbol{\alpha}^r), \quad (27)$$

where $\boldsymbol{\alpha}^s$ and $\boldsymbol{\alpha}^r$ are the phase directions associated with the rays connecting the image point and the source and receiver, respectively (see Figure 5). The right implication is also true, but in the case of multipathing per branch only (see subsection 2.2). This transformation removes the use of the Beylkin determinant (de Hoop, Spencer and Burridge 1999). It also unfolds caustics (de Hoop and Brandsberg-Dahl 2000) through well-defined mappings from the scattering point to the acquisition manifold. The domains of integration then become

$$\partial S\times\partial R \longleftarrow S^s\times S^r \text{ for given } \boldsymbol{x}'. \quad (28)$$

Here S^s and S^r are two unit circles in the symmetry plane for the sources and receivers, respectively. We introduce the extended Jacobian

$$\mathcal{J}(\boldsymbol{\alpha}^r,\boldsymbol{x}',\boldsymbol{\alpha}^s) = |\rho^{(0)}(\boldsymbol{x}')A^{||}(\boldsymbol{x}^s,\boldsymbol{x}')A^{||}(\boldsymbol{x}',\boldsymbol{x}^r)|^2\frac{\partial(\boldsymbol{x}^s,\boldsymbol{x}^r)}{\partial(\boldsymbol{\alpha}^s,\boldsymbol{\alpha}^r)}, \quad (29)$$

and change the coordinates through the mapping in equation (27) in all relevant places in the following. The in-plane geometrical spreading of $A^{||}$ and the Jacobian cancel each other up to projection factors. Using the expression for the extended Jacobian in equation (26) yields

$$\mathbf{Nc}^{(1)}(\boldsymbol{x}') \approx \int_{S^s\times S^r}\int_X\int_{\mathbb{R}} \frac{\omega^3}{|\mathcal{L}^\perp(\boldsymbol{\alpha}^r,\boldsymbol{x}',\boldsymbol{\alpha}^s)|^2}\mathbf{w}(\boldsymbol{\alpha}^r,\boldsymbol{x}',\boldsymbol{\alpha}^s)\mathbf{w}^T(\boldsymbol{\alpha}^r,\boldsymbol{x}',\boldsymbol{\alpha}^s)$$
$$\cdot\,\mathbf{c}^{(1)}(\boldsymbol{x})e^{\mathrm{i}\omega\nabla_{\boldsymbol{x}'}T(\boldsymbol{\alpha}^r,\boldsymbol{x}',\boldsymbol{\alpha}^s)\cdot(\boldsymbol{x}-\boldsymbol{x}')}\mathcal{J}(\boldsymbol{\alpha}^r,\boldsymbol{x}',\boldsymbol{\alpha}^s)\mathrm{d}\omega\mathrm{d}\boldsymbol{x}\mathrm{d}\boldsymbol{\alpha}^s\mathrm{d}\boldsymbol{\alpha}^r. \quad (30)$$

In accordance with the reasoning in subsection 3.1 we write equation (30) as an integral over $\boldsymbol{x}$ and its Fourier dual $\boldsymbol{k} = \omega\nabla_{\boldsymbol{x}'}T$, i.e. in the form of a pseudodifferential operator. We introduce a new frequency $\bar{\omega} = \omega|\nabla_{\boldsymbol{x}'}T|$. Then $\omega\nabla_{\boldsymbol{x}'}T = \bar{\omega}\boldsymbol{\nu}^m$, where $\boldsymbol{\nu}^m = \nabla_{\boldsymbol{x}'}T/|\nabla_{\boldsymbol{x}'}T|$ is the migration dip and is a function of $\boldsymbol{\alpha}^r,\boldsymbol{x}',\boldsymbol{\alpha}^s$. With the appropriate substitution this yields

$$\mathbf{Nc}^{(1)}(\boldsymbol{x}') \approx \int_{S^s\times S^r}\int_X\int_{\mathbb{R}} \frac{|\nabla_{\boldsymbol{x}'}T(\boldsymbol{\alpha}^r,\boldsymbol{x}',\boldsymbol{\alpha}^s)|^{-4}\bar{\omega}^3}{|\mathcal{L}^\perp(\boldsymbol{\alpha}^r,\boldsymbol{x}',\boldsymbol{\alpha}^s)|^2}\mathbf{w}(\boldsymbol{\alpha}^r,\boldsymbol{x}',\boldsymbol{\alpha}^s)\mathbf{w}^T(\boldsymbol{\alpha}^r,\boldsymbol{x}',\boldsymbol{\alpha}^s)$$
$$\cdot\,\mathbf{c}^{(1)}(\boldsymbol{x})e^{\mathrm{i}\bar{\omega}\boldsymbol{\nu}^m(\boldsymbol{\alpha}^r,\boldsymbol{x}',\boldsymbol{\alpha}^s)\cdot(\boldsymbol{x}-\boldsymbol{x}')}\mathcal{J}(\boldsymbol{\alpha}^r,\boldsymbol{x}',\boldsymbol{\alpha}^s)\mathrm{d}\bar{\omega}\mathrm{d}\boldsymbol{x}\mathrm{d}\boldsymbol{\alpha}^s\mathrm{d}\boldsymbol{\alpha}^r. \quad (31)$$

Defining

$$\mu_{LS}(\boldsymbol{\alpha}^r,\boldsymbol{x}',\boldsymbol{\alpha}^s) = \frac{\mathcal{J}(\boldsymbol{\alpha}^r,\boldsymbol{x}',\boldsymbol{\alpha}^s)}{|\nabla_{\boldsymbol{x}'}T(\boldsymbol{\alpha}^r,\boldsymbol{x}',\boldsymbol{\alpha}^s)|^4}, \quad (32)$$

results in the simplified expression

$$\mathbf{Nc}^{(1)}(\boldsymbol{x}') \approx \int_{S^s\times S^r}\int_X\int_{\mathbb{R}} \bar{\omega}^3 \frac{\mu_{LS}(\boldsymbol{\alpha}^r,\boldsymbol{x}',\boldsymbol{\alpha}^s)}{|\mathcal{L}^\perp(\boldsymbol{\alpha}^r,\boldsymbol{x}',\boldsymbol{\alpha}^s)|^2}\mathbf{w}(\boldsymbol{\alpha}^r,\boldsymbol{x}',\boldsymbol{\alpha}^s)\mathbf{w}^T(\boldsymbol{\alpha}^r,\boldsymbol{x}',\boldsymbol{\alpha}^s) \cdot \mathbf{c}^{(1)}(\boldsymbol{x}) e^{\mathrm{i}\bar{\omega}\boldsymbol{\nu}^m\,(\boldsymbol{\alpha}^r,\boldsymbol{x}',\boldsymbol{\alpha}^s)\cdot(\boldsymbol{x}-\boldsymbol{x}')}\mathrm{d}\bar{\omega}\mathrm{d}\boldsymbol{x}\mathrm{d}\boldsymbol{\alpha}^s\mathrm{d}\boldsymbol{\alpha}^r. \quad (33)$$

3.1.2 Migration dip, scattering angle and the leading order contribution

We change variables again, from the phase angles to scattering angle θ, which is the angle between $\boldsymbol{\alpha}^s$ and $\boldsymbol{\alpha}^r$, and the migration dip $\boldsymbol{\nu}^m$ (see Figure 5). The scattering angle follows to be

$$\theta = \theta(\boldsymbol{\alpha}^r,\boldsymbol{x}',\boldsymbol{\alpha}^s) = \arccos(\boldsymbol{\alpha}^s\cdot\boldsymbol{\alpha}^r). \quad (34)$$

To be able to integrate over the migration dip, there is assumed to be no scattering over $\theta = \pi$ so that $\nabla_{\boldsymbol{x}'}\,T \neq 0$ and $\boldsymbol{\nu}^m$ is defined. We have

$$(\boldsymbol{x}',\boldsymbol{\alpha}^s,\boldsymbol{\alpha}^r) \leftrightarrows (\boldsymbol{x}',\boldsymbol{\nu}^m,\theta). \quad (35)$$

In 2.5-D this mapping exists both ways; there is no integration over the azimuth (de Hoop and Brandsberg-Dahl 2000). The domains of integration can now be written as

$$S^s\times S^r \longrightarrow E_{\boldsymbol{\nu}^m}\times E_\theta \text{ for given } \boldsymbol{x}'. \quad (36)$$

Changing all relevant coordinates under the mapping in equation (35) and collecting the integration over the scattering angle θ yields

$$\mathbf{Nc}^{(1)}(\boldsymbol{x}') \approx \int_{E_{\boldsymbol{\nu}^m}}\int_{\mathbb{R}}\int_X \bar{\omega}^3 \left\{\int_{E_\theta}\frac{\mu_{LS}(\boldsymbol{x}',\boldsymbol{\nu}^m,\theta)}{|\mathcal{L}^\perp(\boldsymbol{x}',\boldsymbol{\nu}^m,\theta)|^2} \cdot \mathbf{w}(\boldsymbol{x}',\boldsymbol{\nu}^m,\theta)\mathbf{w}^T(\boldsymbol{x}',\boldsymbol{\nu}^m,\theta)\frac{\partial(\boldsymbol{\alpha}^s,\boldsymbol{\alpha}^r)}{\partial(\boldsymbol{\nu}^m,\theta)}\mathrm{d}\theta\right\}\mathbf{c}^{(1)}(\boldsymbol{x})e^{\mathrm{i}\bar{\omega}\boldsymbol{\nu}^m\cdot(\boldsymbol{x}-\boldsymbol{x}')}\mathrm{d}\boldsymbol{x}\mathrm{d}\bar{\omega}\mathrm{d}\boldsymbol{\nu}^m. \quad (37)$$

We introduce the square matrix (of the dimensionality of $\mathbf{w}$)

$$\Gamma(\boldsymbol{x}',\boldsymbol{\nu}^m) = \frac{1}{2}\int_{E_\theta}\frac{\mu_{LS}(\boldsymbol{x}',\boldsymbol{\nu}^m,\theta)}{|\mathcal{L}^\perp(\boldsymbol{x}',\boldsymbol{\nu}^m,\theta)|^2}\mathbf{w}(\boldsymbol{x}',\boldsymbol{\nu}^m,\theta)\mathbf{w}^T(\boldsymbol{x}',\boldsymbol{\nu}^m,\theta)\frac{\partial(\boldsymbol{\alpha}^s,\boldsymbol{\alpha}^r)}{\partial(\boldsymbol{\nu}^m,\theta)}\mathrm{d}\theta + (\ldots)(\boldsymbol{x}',-\boldsymbol{\nu}^m), \quad (38)$$

where the second term is the same as the first but with $\boldsymbol{\nu}^m$ replaced by $-\boldsymbol{\nu}^m$. This enables us to rewrite equation (37) with positive $\bar{\omega}$ only as

$$\mathbf{Nc}^{(1)}(\boldsymbol{x}') \approx \frac{1}{(2\pi)^2}\int_{E_{\boldsymbol{\nu}^m}}\int_{\mathbb{R}_{\geq 0}}\int_X \bar{\omega}^2 8\pi^2\Gamma(\boldsymbol{x}',\boldsymbol{\nu}^m)\mathbf{c}^{(1)}(\boldsymbol{x})e^{\mathrm{i}\bar{\omega}\boldsymbol{\nu}^m\cdot(\boldsymbol{x}-\boldsymbol{x}')}\bar{\omega}\mathrm{d}\boldsymbol{x}\mathrm{d}\bar{\omega}\mathrm{d}\boldsymbol{\nu}^m. \quad (39)$$

This has now explicitly the form of a pseudodifferential operator with integration over $\boldsymbol{x}$ and its dual $\boldsymbol{k}$ through the identification $\boldsymbol{k} = \bar{\omega}\boldsymbol{\nu}^m$. We recognize here the leading order symbol, $\bar{\omega}^2 8\pi^2\Gamma(\boldsymbol{x}',\boldsymbol{\nu}^m)$, of $\mathbf{N}$. Note the differences when compared with the 3-D case found in de Hoop and Brandsberg-Dahl (2000): the out-of-plane geometrical spreading $\mathcal{L}^\perp$ naturally appears in the leading order symbol of the normal operator in equation (38) combined with the radiation patterns. Also the power of (2π) has been modified in accordance with the stationary phase calculation in 2.5-D.

3.2 Least-Squares Inversion

To leading order, the inverse normal operator composed with the normal operator from the last subsection should yield the identity. The departure from the identitity is due to taking the generalized inverse of and smoother contributions to the normal operator. We denote the generalized inverse of $\mathbf{N}$ by $\langle\mathbf{N}^{-1}\rangle$. The resolution is controlled by $\langle\mathbf{N}^{-1}\rangle\mathbf{N}$. General analysis of the resolution is given by de Hoop *et al* (1999) and for the 2.5-D case by Foss and Ursin (2003).

Note that

$$\frac{1}{(2\pi)^2}\int_{\mathbb{R}_{\geq 0}}\int_{S^1} e^{\mathrm{i}\bar{\omega}\boldsymbol{\nu}^m\cdot(\boldsymbol{x}-\boldsymbol{x}')}\bar{\omega}\mathrm{d}\boldsymbol{\nu}^m\mathrm{d}\bar{\omega} = \delta(\boldsymbol{x}-\boldsymbol{x}'). \quad (40)$$

In view of limited illuminations, the support of $\bar{\omega}$ will be bounded while $\boldsymbol{\nu}^m \in E_{\boldsymbol{\nu}^m} \subset S^1$. Equation (40) becomes a band-limited delta function, $\delta_{BL}(\boldsymbol{x})$ (Bleistein 1984). The kernel of the parametrix of $\mathbf{N}$ (we denote the kernel of $\mathbf{N}$ as $\mathcal{N}$) is found to be

$$\langle \mathcal{N}^{-1} \rangle(\boldsymbol{x}', \boldsymbol{x}) = \frac{1}{(2\pi)^2} \int_{\mathbb{R}\geq 0} \int_{E_{\boldsymbol{\nu}^m}} \bar{\omega}^{-2} \langle 8\pi^2 \Gamma(\boldsymbol{x}', \boldsymbol{\nu}^m) \rangle^{-1} e^{\mathrm{i}\bar{\omega}\boldsymbol{\nu}^m \cdot (\boldsymbol{x} - \boldsymbol{x}')} \bar{\omega} \mathrm{d}\boldsymbol{\nu}^m \mathrm{d}\bar{\omega}. \tag{41}$$

Note that one of the $\bar{\omega}$ variables is placed with the integration variables since $(\bar{\omega}, \boldsymbol{\nu}^m)$ yield polar coordinates in $\boldsymbol{k}$-space. The composition of this kernel and the kernel of the normal operator then becomes

$$\int \langle \mathcal{N}^{-1} \rangle(\boldsymbol{x}', \boldsymbol{y}) \mathcal{N}(\boldsymbol{y}, \boldsymbol{x}) \mathrm{d}\boldsymbol{y} \sim \delta_{BL}(\boldsymbol{x}' - \boldsymbol{x}) + \text{lower order terms}. \tag{42}$$

We replace $\boldsymbol{x}'$ with $\boldsymbol{x}$ in the imaging operator (22). The real part of the composition is symmetric in ω' while the imaginary part is odd and disappears. The integration over ω' then becomes one-sided by taking the real part and multiplying by 2 (de Hoop and Brandsberg-Dahl 2000). Using equation (21) the least-squares estimate of the medium perturbation becomes

$$\begin{aligned}
\hat{\mathbf{c}}^{(1)}(\boldsymbol{x}') &= \langle \mathbf{N}^{-1} \rangle \mathbf{L}^{\star} u(\boldsymbol{x}') \\
&\approx \frac{-1}{(2\pi)^2} \frac{1}{\pi} \mathrm{Re} \Big\{ \int_X d\boldsymbol{x} \int_{\mathbb{R}\geq 0} \bar{\omega}^{-1} \mathrm{d}\bar{\omega} \int_{E_{\boldsymbol{\nu}^m}} \mathrm{d}\boldsymbol{\nu}^m \int_{\partial S \times \partial R} \mathrm{d}\boldsymbol{x}^s \mathrm{d}\boldsymbol{x}^r \int_{\mathbb{R}\geq 0} \mathrm{d}\omega' \langle 8\pi^2 \Gamma(\boldsymbol{x}', \boldsymbol{\nu}^m) \rangle^{-1} \\
&\cdot \sqrt{2\pi} (\mathrm{i}\omega')^{3/2} \rho^{(0)}(\boldsymbol{x}') \frac{(A^{||}(\boldsymbol{x}^s, \boldsymbol{x}') A^{||}(\boldsymbol{x}', \boldsymbol{x}^r))^{\star}}{\mathcal{L}^{\perp}(\boldsymbol{x}^r, \boldsymbol{x}', \boldsymbol{x}^s)^{\star}} \mathbf{w}(\boldsymbol{x}^r, \boldsymbol{x}, \boldsymbol{x}^s) h_m(\boldsymbol{x}^r; \boldsymbol{x}') U_{mn}(\boldsymbol{x}^s, \boldsymbol{x}^r, \omega') h_n(\boldsymbol{x}^s; \boldsymbol{x}') \\
&\cdot e^{\mathrm{i}\bar{\omega}\boldsymbol{\nu}^m \cdot (\boldsymbol{x} - \boldsymbol{x}') - \mathrm{i}\omega' T(\boldsymbol{x}^r, \boldsymbol{x}, \boldsymbol{x}^s)} \Big\}.
\end{aligned} \tag{43}$$

We have introduced the time-Fourier transform $U_{mn}(\boldsymbol{x}^s, \boldsymbol{x}^r, \omega')$ of the data, $u_{mn}(\boldsymbol{x}^s, \boldsymbol{x}^r, t')$. We proceed by Taylor expanding $T(\boldsymbol{x}^s, \boldsymbol{x}, \boldsymbol{x}^r)$ about $\boldsymbol{x}'$ as in equation (24). By the same argument as around equation (26), $\boldsymbol{x}'$ is assumed to be close to $\boldsymbol{x}$ as this yields the largest contribution to the oscillatory integral. The amplitude factors and the radiation patterns are slowly varying and can be considered constant in a small neighbourhood of $\boldsymbol{x}'$. This means that we may substitute $\boldsymbol{x}'$ for $\boldsymbol{x}$ for slowly varying components,

$$\begin{aligned}
\hat{\mathbf{c}}^{(1)}(\boldsymbol{x}') \approx \\
&\frac{-1}{(2\pi)^{3/2}\pi} \mathrm{Re} \Big\{ \int_X \mathrm{d}\boldsymbol{x} \int_{\mathbb{R}\geq 0} \bar{\omega}^{-1} \mathrm{d}\bar{\omega} \int_{E_{\boldsymbol{\nu}^m}} \mathrm{d}\boldsymbol{\nu}^m \int_{\partial S \times \partial R} \mathrm{d}\boldsymbol{x}^s \mathrm{d}\boldsymbol{x}^r \int_{\mathbb{R}\geq 0} \mathrm{d}\omega' \langle 8\pi^2 \Gamma(\boldsymbol{x}', \boldsymbol{\nu}^m) \rangle^{-1} (\mathrm{i}\omega')^{3/2} \\
&\cdot \rho^{(0)}(\boldsymbol{x}') \frac{(A^{||}(\boldsymbol{x}^s, \boldsymbol{x}') A^{||}(\boldsymbol{x}', \boldsymbol{x}^r))^{\star}}{\mathcal{L}^{\perp}(\boldsymbol{x}^r, \boldsymbol{x}', \boldsymbol{x}^s)^{\star}} \mathbf{w}(\boldsymbol{x}^r, \boldsymbol{x}', \boldsymbol{x}^s) h_m(\boldsymbol{x}^r; \boldsymbol{x}') U_{mn}(\boldsymbol{x}^s, \boldsymbol{x}^r, \omega') h_n(\boldsymbol{x}^s; \boldsymbol{x}') \\
&\cdot e^{-\mathrm{i}\omega' T(\boldsymbol{x}^r, \boldsymbol{x}', \boldsymbol{x}^s)} e^{\mathrm{i}(\bar{\omega}\boldsymbol{\nu}^m - \omega' \nabla_{\boldsymbol{x}'} T(\boldsymbol{x}^r, \boldsymbol{x}', \boldsymbol{x}^s)) \cdot (\boldsymbol{x} - \boldsymbol{x}')} \Big\}.
\end{aligned} \tag{44}$$

We observe that the integration over $\boldsymbol{x}$ now becomes a delta function,

$$\begin{aligned}
&\int_X \mathrm{d}\boldsymbol{x} e^{\mathrm{i}(\bar{\omega}\boldsymbol{\nu}^m - \omega' \nabla_{\boldsymbol{x}'} T(\boldsymbol{x}^r, \boldsymbol{x}', \boldsymbol{x}^s)) \cdot (\boldsymbol{x} - \boldsymbol{x}')} \\
&\qquad = 4\pi^2 \delta(\bar{\omega}\boldsymbol{\nu}^m - \omega' \nabla_{\boldsymbol{x}'} T(\boldsymbol{x}^r, \boldsymbol{x}', \boldsymbol{x}^s)) = 4\pi^2 \delta(\bar{\omega}\boldsymbol{\nu}^m - \omega' \boldsymbol{\nu}^m |\nabla_{\boldsymbol{x}'} T(\boldsymbol{x}^r, \boldsymbol{x}', \boldsymbol{x}^s)|),
\end{aligned} \tag{45}$$

since $\boldsymbol{\nu}^m = \nabla_{\boldsymbol{x}'} T / |\nabla_{\boldsymbol{x}'} T|$. Using that $\bar{\omega} = \omega |\nabla_{\boldsymbol{x}'} T|$ and the result in equation (44), the integration over $\bar{\omega}$ and $\boldsymbol{\nu}^m$ collapses to

$$\begin{aligned}
\hat{\mathbf{c}}^{(1)}(\boldsymbol{x}') \approx \frac{-\sqrt{2\pi}}{\pi} \mathrm{Re} \Big\{ &\int_{\partial S \times \partial R} \mathrm{d}\boldsymbol{x}^s \mathrm{d}\boldsymbol{x}^r \int_{\mathbb{R}\geq 0} \frac{\mathrm{d}\omega'}{(\omega' |\nabla_{\boldsymbol{x}'} T(\boldsymbol{x}^r, \boldsymbol{x}', \boldsymbol{x}^s)|)^2} \langle 8\pi^2 \Gamma(\boldsymbol{x}', \boldsymbol{\nu}^m) \rangle^{-1} (\mathrm{i}\omega')^{3/2} \\
&\cdot \rho^{(0)}(\boldsymbol{x}') \frac{(A^{||}(\boldsymbol{x}^s, \boldsymbol{x}') A^{||}(\boldsymbol{x}', \boldsymbol{x}^r))^{\star}}{\mathcal{L}^{\perp}(\boldsymbol{x}^r, \boldsymbol{x}', \boldsymbol{x}^s)^{\star}} \mathbf{w}(\boldsymbol{x}^s, \boldsymbol{x}', \boldsymbol{x}^r) h_m(\boldsymbol{x}^r; \boldsymbol{x}') U_{mn}(\boldsymbol{x}^s, \boldsymbol{x}^r, \omega') h_n(\boldsymbol{x}^s; \boldsymbol{x}') \\
&\cdot e^{-\mathrm{i}\omega' T(\boldsymbol{x}^r, \boldsymbol{x}', \boldsymbol{x}^s)} \Big\}.
\end{aligned} \tag{46}$$

Taking 8π out of the generalized inverse and making the appropriate changes yields

$$\begin{aligned}
\hat{\mathbf{c}}^{(1)}(\boldsymbol{x}') \approx \frac{1}{(2\pi)^{5/2}} \mathrm{Re} \Big\{ &\int_{\partial S \times \partial R} \mathrm{d}\boldsymbol{x}^s \mathrm{d}\boldsymbol{x}^r \int_{\mathbb{R}\geq 0} \frac{\mathrm{d}\omega'}{(\omega' \mathrm{i})^{1/2} |\nabla_{\boldsymbol{x}'} T(\boldsymbol{x}^r, \boldsymbol{x}', \boldsymbol{x}^s)|^2} \langle \Gamma(\boldsymbol{x}', \boldsymbol{\nu}^m) \rangle^{-1} \\
&\cdot \rho^{(0)}(\boldsymbol{x}') \frac{(A^{||}(\boldsymbol{x}^s, \boldsymbol{x}') A^{||}(\boldsymbol{x}', \boldsymbol{x}^r))^{\star}}{\mathcal{L}^{\perp}(\boldsymbol{x}^r, \boldsymbol{x}', \boldsymbol{x}^s)^{\star}} \mathbf{w}(\boldsymbol{x}^r, \boldsymbol{x}', \boldsymbol{x}^s) h_m(\boldsymbol{x}^r; \boldsymbol{x}') U_{mn}(\boldsymbol{x}^s, \boldsymbol{x}^r, \omega') h_n(\boldsymbol{x}^s; \boldsymbol{x}') \\
&\cdot e^{-\mathrm{i}\omega' T(\boldsymbol{x}^r, \boldsymbol{x}', \boldsymbol{x}^s)} \Big\}.
\end{aligned} \tag{47}$$

(Equation (47) is in fact a direct manifestation of the composition of a pseudodifferential operator with a FIO (Treves 1980, Section 6.1. Chapter VIII)). The surface coordinates $\boldsymbol{x}^r$ and $\boldsymbol{x}^s$ are changed to the phase directions at the scattering point as in relation (27). Using equation (29) and (32), the appropriate Jacobian can be expressed as

$$\frac{\partial(\boldsymbol{x}^s,\boldsymbol{x}^r)}{\partial(\boldsymbol{\alpha}^s,\boldsymbol{\alpha}^r)} = \frac{\mu_{LS}(\boldsymbol{\alpha}^r,\boldsymbol{x}',\boldsymbol{\alpha}^s)|\nabla_{\boldsymbol{x}'}T(\boldsymbol{x}^r,\boldsymbol{x}',\boldsymbol{x}^s)|^4}{|\rho^{(0)}(\boldsymbol{x}')A^{||}(\boldsymbol{x}^s,\boldsymbol{x}')A^{||}(\boldsymbol{x}',\boldsymbol{x}^r)|^2}. \tag{48}$$

Inserting the result in equation (47) yields the estimate of the medium perturbation

$$\hat{\mathbf{c}}^{(1)}(\boldsymbol{x}') \approx \frac{1}{(2\pi)^{5/2}}\mathrm{Re}\Big\{ \int_{S^s\times S^r}\mathrm{d}\boldsymbol{\alpha}^s\,\mathrm{d}\boldsymbol{\alpha}^r \int_{\mathbb{R}\geq 0}\frac{\mathrm{d}\omega'}{(\omega'\mathrm{i})^{1/2}}\mu_{LS}(\boldsymbol{\alpha}^r,\boldsymbol{x}',\boldsymbol{\alpha}^s)\langle\Gamma(\boldsymbol{x}',\boldsymbol{\nu}^m)\rangle^{-1}$$
$$\cdot\frac{|\nabla_{\boldsymbol{x}'}T(\boldsymbol{\alpha}^r,\boldsymbol{x}',\boldsymbol{\alpha}^s)|^2\mathbf{w}(\boldsymbol{\alpha}^r,\boldsymbol{x}',\boldsymbol{\alpha}^s)h_m(\boldsymbol{x}^r;\boldsymbol{x}')U_{mn}(\boldsymbol{x}^s,\boldsymbol{x}^r,\omega')h_n(\boldsymbol{x}^s;\boldsymbol{x}')}{\rho^{(0)}(\boldsymbol{x}')A^{||}(\boldsymbol{\alpha}^s,\boldsymbol{x}')A^{||}(\boldsymbol{x}',\boldsymbol{\alpha}^r)\mathcal{L}^{\perp}(\boldsymbol{\alpha}^r,\boldsymbol{x}',\boldsymbol{\alpha}^s)^{\star}}e^{-\mathrm{i}\omega' T(\boldsymbol{\alpha}^r,\boldsymbol{x}',\boldsymbol{\alpha}^s)}\Big\}. \tag{49}$$

We observe in the denominator the out-of-plane geometrical spreading, which also exists in the expression for Γ (equation (38)). Changing the variables from phase angles to scattering angle θ and migration dip $\boldsymbol{\nu}^m$ as in (35) yields

$$\hat{\mathbf{c}}^{(1)}(\boldsymbol{x}') \approx \frac{1}{(2\pi)^{5/2}}\mathrm{Re}\Big\{ \int_{E_{\boldsymbol{\nu}^m}\times E_\theta}\mathrm{d}\theta\mathrm{d}\boldsymbol{\nu}^m\frac{\partial(\boldsymbol{\alpha}^s,\boldsymbol{\alpha}^r)}{\partial(\boldsymbol{\nu}^m,\theta)}\int_{\mathbb{R}\geq 0}\frac{\mathrm{d}\omega'}{(\omega'\mathrm{i})^{1/2}}\mu_{LS}(\boldsymbol{x}',\boldsymbol{\nu}^m,\theta)\langle\Gamma(\boldsymbol{x}',\boldsymbol{\nu}^m)\rangle^{-1}$$
$$\cdot\frac{|\nabla_{\boldsymbol{x}'}T(\boldsymbol{x}',\boldsymbol{\nu}^m,\theta)|^2\mathbf{w}(\boldsymbol{x}',\boldsymbol{\nu}^m,\theta)h_m(\boldsymbol{x}^r;\boldsymbol{x}')U_{mn}(\boldsymbol{x}^s,\boldsymbol{x}^r,\omega')h_n(\boldsymbol{x}^s;\boldsymbol{x}')}{\rho^{(0)}(\boldsymbol{x}')A^{||}(\boldsymbol{x}^s,\boldsymbol{x}')A^{||}(\boldsymbol{x}',\boldsymbol{\alpha}^r)\mathcal{L}^{\perp}(\boldsymbol{x}',\boldsymbol{\nu}^m,\theta)^{\star}}e^{-\mathrm{i}\omega' T(\boldsymbol{x}',\boldsymbol{\nu}^m,\theta)}\Big\}, \tag{50}$$

where we have left the phase directions in the argument of the in-plane amplitudes to distinguish them. The Jacobian inside the integral can be found in (Burridge *et al.* 1998). The integral over migration dip makes this an inverse by generalized Radon transform (GRT).

4 TRANSFORMATION INTO ANGLE GATHERS

When constructing angle gathers we fix the scattering angle, θ, and integrate over the migration dip, $\boldsymbol{\nu}^m$. The restriction can introduce artifacts in the angle gathers when the medium is inhomogeneous (i.e. in the presence of caustics) due to multipathing in the recorded wave-field. These artifacts are different from the artifacts due to the failure of assumption 3. These artifacts are not present in the inversion by equation (50) since they stack destructively (Stolk and de Hoop 2002).

Since the restriction to a fixed scattering angle means that we no longer stack over all the data, but rather over subsets of the data that change with image point and scattering angle, we reintroduce $\boldsymbol{x}^s$ and $\boldsymbol{x}^r$ as the variables of integration. This requires the notion of branches of the two-way travel time (see equation (10)). We define $\theta^{(i)}$ as $\theta(\boldsymbol{\alpha}^r,\boldsymbol{x}',\boldsymbol{\alpha}^s)$ (cf. (34)-(35)) composed with the inverse of map (27), associating the scattering angle with the acquisition coordinates $\boldsymbol{x}^s,\boldsymbol{x}^r$. We define the 'angle' transform $\mathbf{K}$ (the GRT) via a restriction of the imaging operator $\mathbf{L}^\star$ in equation (22) to fixed angle $\theta^{(i)}=\theta'$, where $i\in I$ indexes the travel time branch. We reintroduce the sum over the different travel time branches suppressed since equation (9). Thus we multiply the kernel of $\mathbf{L}^\star$ in equation (22) by a delta function, $\delta(\theta^{(i)}-\theta')$. The kernel of $\mathbf{K}$, denoted by $\mathcal{K}_{mn}$, can be written as an oscillatory integral (after a change of $\boldsymbol{x}'$ to $\boldsymbol{x}$)

$$\mathcal{K}_{mn}(\boldsymbol{x},\theta',\boldsymbol{x}^s,\boldsymbol{x}^r,t) = \sum_{i\in I}(2\pi\sqrt{\mathrm{i}})^{-1}\int\omega'^{3/2}\rho^{(0)}(\boldsymbol{x})$$
$$\cdot\frac{(A^{||}(\boldsymbol{x}^s,\boldsymbol{x})A^{||}(\boldsymbol{x},\boldsymbol{x}^r))^{\star}}{\mathcal{L}^{\perp}(\boldsymbol{x}^r,\boldsymbol{x},\boldsymbol{x}^s)^{\star}}\mathbf{w}(\boldsymbol{x}^r,\boldsymbol{x},\boldsymbol{x}^s)h_m(\boldsymbol{x}^r;\boldsymbol{x})h_n(\boldsymbol{x}^s;\boldsymbol{x})e^{-\mathrm{i}\Phi^{(i)}(\boldsymbol{x},\boldsymbol{x}^r,\boldsymbol{x}^s,t,\theta',\omega',\varepsilon)}\mathrm{d}\omega'\mathrm{d}\varepsilon. \tag{51}$$

Here ε is the Fourier dual of the scattering angle θ (Stolk and de Hoop 2002) and

$$\Phi^{(i)}(\boldsymbol{x},\boldsymbol{x}^r,\boldsymbol{x}^s,t,\theta',\omega',\varepsilon) = \omega'[T^{(i)}(\boldsymbol{x}^r,\boldsymbol{x},\boldsymbol{x}^s)-t]+\varepsilon[\theta'-\theta^{(i)}(\boldsymbol{x}^r,\boldsymbol{x},\boldsymbol{x}^s)]. \tag{52}$$

The artifacts of the restriction can be evaluated by considering the composition $\mathbf{KL}$, a θ'-family of operators each member of which resembles the normal operator. The artifacts in the angle gathers can be recognized by their 'move-out' in angle. A multi-dimensional filter in the Fourier domain (see equation (51)) can be applied to remove the artifacts associated with $|\varepsilon|\geq\varepsilon_0>0$. Brandsberg-Dahl *et al.* (2003b) suppressed the artifacts by so-called *focusing in dip*.

By proceeding as suggested above using the appropriate changes of variables leading up to equation (50), the angle depen-

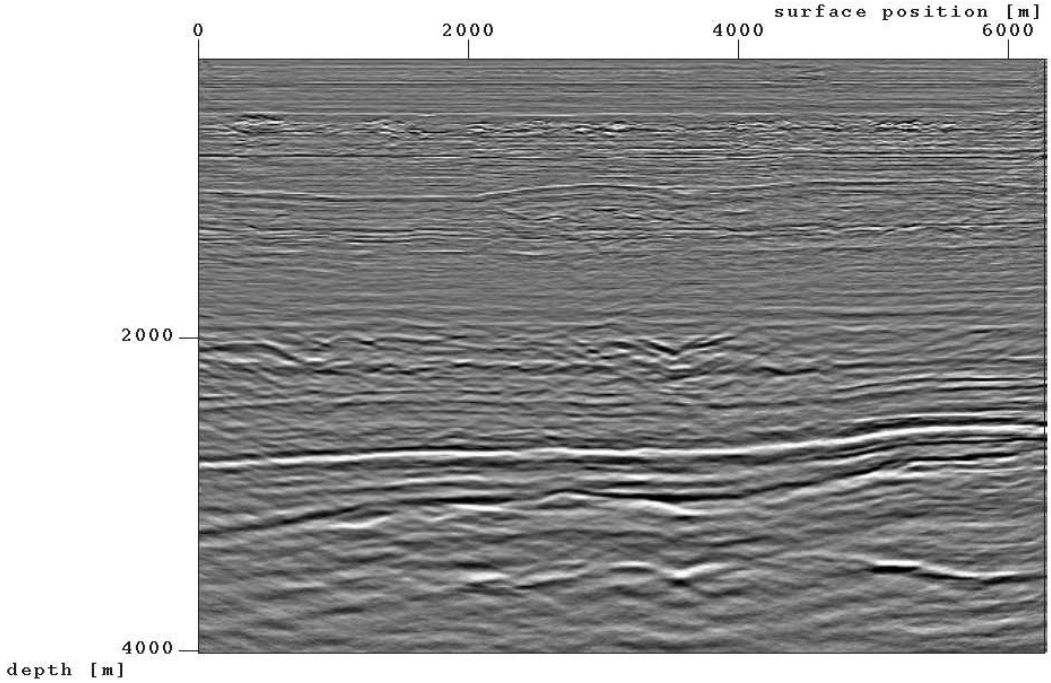

Figure 6. Image created as a linear combination of inverted parameters from equation (50) using PP-scattering event of the North Sea (OBC) data set.

dent parameter estimates (used to construct common-image point gathers) are given by

$$\hat{\mathbf{c}}^{(1)}(\boldsymbol{x}';\theta') \approx \frac{1}{(2\pi)^{5/2}}\mathrm{Re}\left\{\int_{E_{\boldsymbol{\nu}^m}} \mathrm{d}\boldsymbol{\nu}^m \frac{\partial(\boldsymbol{\alpha}^s,\boldsymbol{\alpha}^r)}{\partial(\boldsymbol{\nu}^m,\theta')}\int_{\mathbb{R}\geq 0}\frac{\mathrm{d}\omega'}{(\omega'\mathrm{i})^{1/2}}\mu_{LS}(\boldsymbol{x}',\boldsymbol{\nu}^m,\theta')\langle\Gamma(\boldsymbol{x}',\boldsymbol{\nu}^m)\rangle^{-1}\right.$$
$$\left.\cdot\frac{|\nabla_{\boldsymbol{x}'}T(\boldsymbol{x}',\boldsymbol{\nu}^m,\theta')|^2\mathbf{w}(\boldsymbol{x}',\boldsymbol{\nu}^m,\theta')h_m(\boldsymbol{x}^r;\boldsymbol{x}')U_{mn}(\boldsymbol{x}^s,\boldsymbol{x}^r,\omega')h_n(\boldsymbol{x}^s;\boldsymbol{x}')}{\rho^{(0)}(\boldsymbol{x}')A^{||}(\boldsymbol{\alpha}^s,\boldsymbol{x}')A^{||}(\boldsymbol{x}',\boldsymbol{\alpha}^r)\mathcal{L}^{\perp}(\boldsymbol{x}',\boldsymbol{\nu}^m,\theta')^{\star}}e^{-\mathrm{i}\omega'T(\boldsymbol{x}',\boldsymbol{\nu}^m,\theta')}\right\}. \quad (53)$$

Note that we again have suppressed the summation of the travel time branches. The factor $\Gamma(\boldsymbol{x}',\boldsymbol{\nu}^m)$ is an average in θ of the radiation patterns. $\langle\Gamma(\boldsymbol{x}',\boldsymbol{\nu}^m)\rangle^{-1}$ then acts as a least-squares (LS) removal of the radiation patterns. This is hence a LS-AVA-compensated parameter estimate. Since, upon filtering, $\hat{\mathbf{c}}^{(1)}(\boldsymbol{x}';\theta')$ should only depend smoothly on θ' if the correct background medium is used, the detection of smoothness can be used as a criterion for velocity analysis. Brandsberg-Dahl *et al.* (2003a) followed such an angle tomographic approach to determine the background medium.

5 EXAMPLE

Here we give an example using real data from the North Sea. The data set is acquired using ocean bottom cable (OBC) acquisition. We use data from a single ocean bottom cable making the intersection of a presumed symmetry plane and the ocean bottom.

Using equation (50) we perform an isotropic inversion considering PP-scattering events and an isotropic background medium. This yields information on the three independent parameter perturbations $\rho^{(1)}$, $c^{(1)}_{1111}$ and $c^{(1)}_{1133}$ in equation (15). An image is created as a linear combination of these parameters given in Figure 6. The geology varies mostly in the imaging plane making this an accurate 2.5-D problem under our assumptions 1 and 2. However, at depths greater than 3000 meters, the 2.5-D framework deteriorates. By this we mean that the geology also varies significantly in the out-of-plane direction sending energy out of the computational plane. Hence, sufficient information on the reflectors here is simply not contained in our data (the single acquisition cable data set). The top part of Figure 7 is a high resolution detail from Figure 6, with surface position from 3000 to $4000\,m$ and depth from 1850 to $2150\,m$. The V-shape in the lower part of the image is a distinct geological feature believed to be either a slump fault or an erosive channel deposit. As a slump fault the left part of the V-shape has dropped and new layers have deposited on the slope created. The lower part of the figure is a schematic drawing of the feature as an erosive channel, where water has dug into

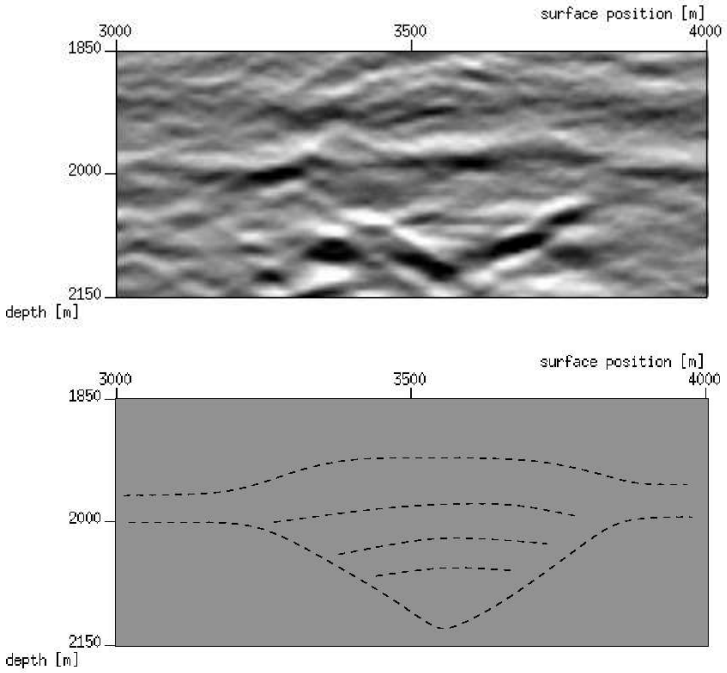

Figure 7. Top figure is a high resolution image of detail from Figure 6. The image shows a possible slump fault or erosive channel deposit. Their dominant features are captured in this 2-D slice. The bottom figure is a schematic drawing of the image as an erosive channel deposit.

the horizontal layer and new material has deposited later leaving a slight curve in the layer, the V-shape. Both of these geological features have a slowly varying behavior in one direction. Given that our computational plane is intersecting at the right angle, the main features are described by this slice and the smoothly varying behavior are in the out-of-plane direction. Hence the 2.5-D framework applies with decent accuracy.

Figure 8 shows LS-AVA-compensated common-image point gathers for PP- and PS-scattering events, respectively, created as a combination of the parameters from equation (53) at surface position $x_1 = 1500\ m$. The combinations are chosen as the appropriate acoustic impedances; i.e. P-wave impedance for the PP-gather and S-wave impedance for the PS-gather. The vertical scale is from $800\ m$ to $3200\ m$ in depth. Following convention, both common-image point gathers are plotted as functions of incoming P-wave angle, ranging from 0 to 35 degrees. Note that the zero angle contribution of the PS-gather is set to zero as this is not defined. Only a subset of the reflectors are comparable in depth between PP- and PS-gathers, yet with very different strength in amplitudes. As mentioned, the imaging is done in an isotropic smooth background medium, yet the medium is anisotropic. The anisotropy has a strong effect on the travel times and thus the depths. This can explain why certain reflectors, when comparing the two common-image point gathers, seem to be at different depths. Note that the amplitude behavior is close to constant with angle. Hence, for this range of scattering angles, the LS-AVA-compensation in equation (53) suppresses the amplitude behavior. This is important in angle tomography through the use of 'differential semblance' (Brandsberg-Dahl *et al.* 2003a). It is clear from this example, that a joint treatment of (q)P and (q)S velocities becomes necessary in reflection tomography.

6 DISCUSSION

This paper presents the general form of 2.5-D modeling, imaging-inversion and AVA-compensated angle transform formulas in anisotropic elastic media under necessary and sufficient assumptions. The results extend those of Bleistein (1986) to the cases of multipathing and anisotropic elasticity. Assumption 1 restricts us to a monoclinic medium as the lowest possible symmetry. However, under the addition of assumption 2, the wave propagation is restricted to the plane. Any symmetries lower than a transversely isotropic medium with the symmetry axis contained in the plane of consideration have to be excluded for the purpose of inversion and reflection tomography.

In the presence of caustics, artifacts may be generated by the imaging-inversion procedures. Subject to the Bolker condition such artifacts are avoided. We have made the observation that the 2-D Bolker condition in the symmetry plane implies the Bolker condition in three dimensions in the framework of the common azimuth acquisition geometry. Artifacts in the common image-point

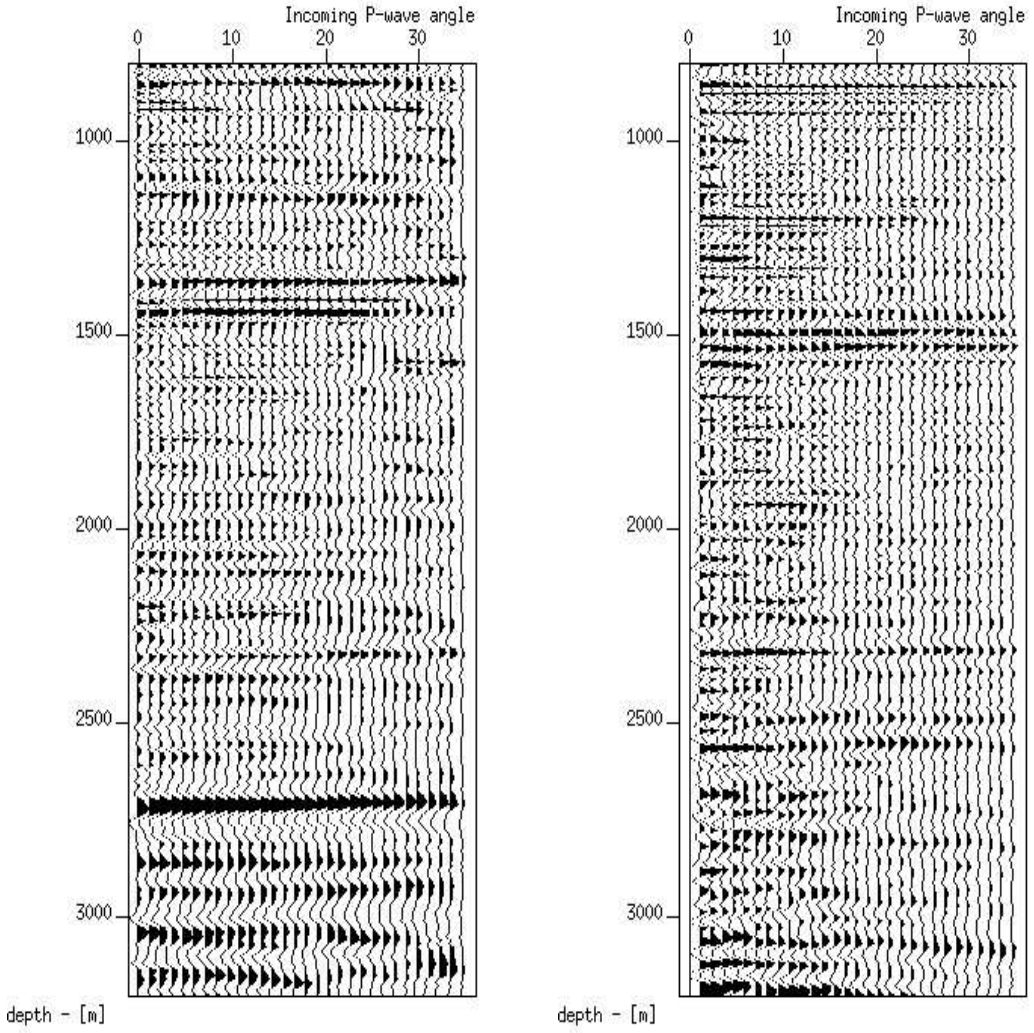

Figure 8. LS-AVA-compensated common-image point gathers for PP- and PSV-scattering, respectively at surface position $1500\,m$ in Figure 6 created using equation (53). The depth range is from 800 to $3200\,m$. Both common-image point gathers are plotted as functions of incoming P-wave angle, from 0 to 35 degrees.

gathers are also controlled by the ray geometry in the symmetry plane only and can thus be filtered out by 2-D considerations. An interesting aspect of our results is the appearance of out-of-plane contributions, by the geometrical spreading, contained naturally in the least-squares removal of the radiation patterns. Intuitively this can be understood as the removal of the stationary contribution to the radiation patterns from the out-of-plane geometrical spreading.

The primary applications of our 2.5-D formulation are a slicewise approach to (i) time-lapse seismics, and (ii) reflection tomography. We elaborate on the second application. The new least-squares AVA-compensated transform of seismic data into common-image point gathers in anisotropic media enables a slicewise approach to migration velocity analysis. This is a better compensation of the AVA-effects than by a pointwise removal as found in (Brandsberg-Dahl *et al.* 2003a). Given a medium that has its dominant change in two directions we may invoke the 2.5-D assumptions approximately to slices in the smoothly varying direction as done in the example, section 5. We parametrize the medium in a finite dimensional subspace of possible smooth background models by a collection of slices $\underline{\mathbf{m}} = \{\mathbf{m}(x_2)\}$, for all values of x_2 under consideration, where each $\mathbf{m}(x_2)$ is the 2-D parametrization of a slice at x_2. Angle tomography (Brandsberg-Dahl *et al.* 2003a) can be done per slice by differential semblance (Symes and Carazzone 1991) on AVA-compensated common-image point gathers generated by equation (53). We extend this by

applying the appropriate out-of-plane 'annihilator' as a Tikhonov regularizer to the misfit functional

$$J[\underline{\mathbf{m}}] = \frac{1}{2}\int\Big\{\int\int\Big|\left[\partial_\theta - (\partial_\theta \Xi(\boldsymbol{x},\theta,x_2))\Xi(\boldsymbol{x},\theta,x_2)^{-1}\right]\hat{\mathbf{c}}^{(1)}[\underline{\mathbf{m}}](\boldsymbol{x};\theta,x_2)\Big|^2\,\mathrm{d}\boldsymbol{x}\mathrm{d}\theta + \lambda\int\left|\partial_{x_2}^2\mathbf{c}^{(0)}[\underline{\mathbf{m}}](\boldsymbol{x},x_2)\right|^2\mathrm{d}\boldsymbol{x}\Big\}\mathrm{d}x_2, \quad (54)$$

where (cf. equation (38))

$$\Xi(\boldsymbol{x},\theta,x_2) = \frac{\mu_{LS}(\boldsymbol{x},\boldsymbol{\nu}^m,\theta)}{|\mathcal{L}^\perp(\boldsymbol{x},\boldsymbol{\nu}^m,\theta)|^2}\frac{\partial(\boldsymbol{\alpha}^s,\boldsymbol{\alpha}^r)}{\partial(\boldsymbol{\nu}^m,\theta)}\langle\Gamma(\boldsymbol{x},\boldsymbol{\nu}^m)\rangle^{-1}\mathbf{w}(\boldsymbol{x},\boldsymbol{\nu}^m,\theta)\mathbf{w}^T(\boldsymbol{x},\boldsymbol{\nu}^m,\theta). \quad (55)$$

All relevant parameters of equation (55) are calculated for $\boldsymbol{\nu}^m$ in the wavefront set of $\hat{\mathbf{c}}^{(1)}$. $\mathbf{c}^{(0)}[\underline{\mathbf{m}}](\boldsymbol{x},x_2)$ is a vector of the parameters of the background medium given the current parametrization $\underline{\mathbf{m}}$. λ in equation (54) is a statistical quantity controlling the trade-off between in-plane and out-of-plane fit (Tenorio 2001) and $\boldsymbol{x} = (x_1, x_3)$. ∂_θ and ∂_{x_2} are the partial derivatives with respect to the scattering angle and out-of-plane coordinate, respectively. The LS-AVA-compensated inversion result from equation (53) is denoted $\hat{\mathbf{c}}^{(1)}[\underline{\mathbf{m}}](\boldsymbol{x};\theta,x_2)$ to emphasize that it is generated using the current parametrization of the smooth background model, $\underline{\mathbf{m}}$, for the slice at out-of-plane coordinate x_2. The minimum of this function indicates a smooth background model such that the data are in the range of the 2.5-D modelling operator. In this way the 2.5-D framework provides a fast computational tool for 3-D tomography and an increased ability to monitor the regularization of the search for a fitting model.

ACKNOWLEDGMENTS

Stig-Kyrre Foss would like to thank the Center for Wave Phenomena, Colorado School of Mines for the opportunity to stay as a guest from Fall 2001 to Summer 2002. He would also like to thank the URE-project, NTNU, Trondheim, Norway for financial support, and Sverre Brandsberg-Dahl for the use of Figure 3. The authors thank Statoil for the use of the North Sea data, Børge Arntsen for data handling and Barbara McLenon for her help preparing the manuscript.

REFERENCES

Beylkin, G., 1985. Imaging the discontinuities in the inverse scattering problem by inversion of a causal generalized Radon transform, *J. Math. Phys.*, **26**, 99-108.

Beylkin, G. and Burridge, R., 1990. Linearized inverse scattering problems in acoustics and elasticity, *Wave Motion*, **12**, 15-52.

Billette, F. and Lambar´e, G., 1998. Velocity macro model estimation from seismic reflection sata by Stereotomography, *Geoph. J. Int.*, **135**, 671-680.

Biondi, B. and Palacharla, G., 1996. 3-D prestack migration of common-azimuth data, *Geophysics*, **61**, 1822-1832.

Bleistein, N. , 1984. Mathematics of wave phenomena, *Academic Press Inc., New York*.

Bleistein, N. , 1986. Two-and-one-half dimensional in-plane wave propagation, *Geoph. Prosp.*, **34**, 686-703.

Bostock, M. G., Rondenay, S., and Shragge, J., 2001. Multiparameter two-dimensional inversion of scattered teleseismic body waves: 1. Theory for oblique incidence, *J. Geophys. Res.*, **106**, 30771-30782.

Brandsberg-Dahl, S., Ursin, B. and de Hoop, M.V., 2003a. Seismic velocity analysis in the scattering-angle/azimuth domain, *Geophys. Prosp.*, in print.

Brandsberg-Dahl, S., de Hoop, M.V., and Ursin, B., 2003b. Focusing in dip and AVA compensation on scattering-angle/azimuth common image gathers, *Geophysics*, **68**, 232-254.

Burridge, R., de Hoop, M.V., Miller, D. and Spencer, C., 1998. Multiparameter inversion in anisotropic elastic media, *Geophys. J. Int.*, **134**, 757-777.

Červen´y, V., 1981. Computation of geometrical spreading by dynamic ray tracing, *Stanford University: SEP-28*, 61-73.

Červen´y, V., 2001. Seismic Ray Theory, *Cambridge University Press, Cambridge*.

Chapman, C. H. and Pratt, R. G., 1992, Traveltime tomography in anisotropic media-I. Theory, *Geophys. J. Int.*, **109**, 1-19.

de Hoop, M.V. and Brandsberg-Dahl, S., 2000. Maslov asymptotic extension of generalized Radon transform inversion in anisotropic elastic media: A least-squares approach, *Inverse Problems*, **16**, 519-562.

de Hoop, M.V. and de Hoop, A.T., 2000. Wavefield reciprocity and local optimization in remote sensing, *Proc. R. Soc. Lond. A*, **456**, 641-682.

de Hoop, M.V., Spencer, C. and Burridge, R., 1999. The resolving power of seismic amplitude data: An anisotropic inversion/migration approach, *Geophysics*, **64**, 852-873.

de Hoop, M.V., Malcolm, A.E. and Le Rousseau, J.H., 2002. Seismic wavefield continuation in the single scattering approximation: A framework for dip and azimuth moveout, *Can. Appl. Math. Q.*, in print.

de Hoop, M.V., Le Rousseau, J. H. and Biondi, B., 2003. Symplectic structure of wave-equation imaging: A path-integral approach based on the double-square-root equation, *Geophys. J. Int.*, **153**, 52-74.

Dellinger, J.A., Gray, S.H., Murphy, G.E. and Etgen, J.T., 2000. Efficient 2.5-D true-amplitude migration, *Geophysics*, **65**, 943-950.

Duistermaat, J.J., 1996. Fourier integral operators, *Birkhäuser, Boston*.

Ettrich, N., Sollid, A. and Ursin, B., 2002. Out-of-plane geometrical spreading in anisotropic media, *Geoph. Prosp.*, **50**, 383-392.

Foss, S. K. and Ursin, B., 2003. 2.5-D modeling, inversion and angle migration in anisotropic elastic media, *Geophys. Prosp.*, submitted.

Geoltrain, S., 1989. Asymptotic solutions to direct and inverse scattering in anisotropic media, *Ph.d. thesis: Colorado School of Mines, Golden*.

Goldin, S. V., 1986. Seismic traveltime inversion, *SEG: Investigations in Geophysics No. 1*.

Guillemin, V., 1985. On some results of Gelfand in integral geometry, *Proceedings of Symposia in Pure Mathematics, American Mathematical Society*, **43**, 149-155.

Hansen, S., 1991. Solution of a hyberbolic inverse problem by linearization, *Comm. Partial Differential Equations*, **16**, 291-309.

Hörmander, L., 1985a. *The analysis of linear partial diferential operators*, Vol. 3, *Springer-Verlag, Berlin*.

Klimeš, L., 1997. Phase shift of the Green function due to caustics in anisotropic media, Expanded Abstracts, 68th Ann. Internat. Mtg., *Soc. Explor. Geophys.*, , 1834-1837.

Miller, D., Oristaglio, M. and Beylkin, G., 1987. A new slant on seismic imaging: migration and integral geometry, *Geophysics*, **52**, 943-964.

Musgrave, M.J.P., 1970. Crystal Acoustics, *Holden-Day, San Francisco*.

Nolan, C. J. and Symes, W. W. 1997. Global solution of a linearized inverse problem for the wave equation. *Comm. Partial Differential Equations*, **22**, 919-952.

Rakesh, 1988. A linearised inverse problem for the wave equation, *Comm. in Part. Diff. Eqs.*, **13**, 573-601.

Sollid, A. and Ursin, B., 2003. Scattering-angle migration of OBS data in weakly anisotropic media, *Geophysics*, **68**, 641-655.

Stolk, C.C., 2000. Microlocal analysis of a seismic linearized inverse problem, *Wave Motion*, **32**, 267-290.

Stolk, C.C. and de Hoop, M.V., 2002. Microlocal analysis of seismic inverse scattering in anisotropic elastic media, *Communications in Pure and Applied Mathematics*, **55**, 261-301.

Symes, W. and Carazzone, J., 1991.Velocity inversion by differential semblance optimization, *Geophysics*, **56**, 654-663.

Ten Kroode, A. P. E., Smit, D. J. and Verdel, A. R., 1998. A microlocal analysis of migration, *Wave Motion*, **28**, 149-172.

Tenorio, L., 2001. Statistical regularization of inverse problems, *SIAM review*, **43**, 347-366.

Thomsen, L., 1986. Weak elastic anisotropy, *Geophysics*, **51**, 1954-1966.

Treves, F., 1980. Introduction to pseudodifferential and Fourier integral operators, *Plenum Press, New York*, **1**.

Tygel, M., Schleicher, J., Hubral, P. and Santos, L.T., 1998. 2.5-D true-amplitude Kirchhoff migration to zero offset in laterally inhomogeneous media, *Geophysics*, **63**, 557-573.

Ursin, B., 2003. Parameter inversion and angle migration in anisotropic elastic media, *Geophysics*, submitted.

APPENDIX A: THE 2.5-D BORN MODELLING FORMULA

The 3-D Born formula is a high frequency approximation to the fi eld scattered off the medium perturbation at $\boldsymbol{x} \in \mathbb{R}^3$, collected at the receiver position $\boldsymbol{x}^r$ generated by a source at $\boldsymbol{x}^s$. This fi eld is calculated by substituting the appropriate GRA Green's functions (2) in the Born approximation. It gives that, under assumption 1 on the medium, the m-direction of the scattered fi eld at the receiver position $\boldsymbol{x}^r$ due to a n-component source at $\boldsymbol{x}^s$ written as a Fourier integral operator is

$$U_{mn}(\boldsymbol{x}^r, \boldsymbol{x}^s, \omega) \approx \int_X \left\{ \int_{\mathbb{R}} \omega^2 h_m(\boldsymbol{x}^r) \rho^{(0)}(\boldsymbol{x}) A(\boldsymbol{x}^s, \boldsymbol{x}) A(\boldsymbol{x}, \boldsymbol{x}^r) \mathbf{w}^T(\boldsymbol{x}^r, \boldsymbol{x}, \boldsymbol{x}^s) e^{\mathrm{i}\omega T(\boldsymbol{x}^r, \boldsymbol{x}, \boldsymbol{x}^s)} h_n(\boldsymbol{x}^s) \mathrm{d}x_2 \right\} \cdot \mathbf{c}^{(1)}(x_1, x_3) \mathrm{d}x_1 \mathrm{d}x_3. \quad \text{(A1)}$$

The medium perturbation $\mathbf{c}^{(1)}$ and the radiation patterns $\mathbf{w}$ are, for the lowest possible symmetry (triclinic), 22×1-matrices of the form as in equations (15) and (16), respectively. The domain of integration of the (x_1, x_3)-coordinates, X, is defi ned in subsection 2.2.

Upon scaling, $x_2 = \tilde{x}_2/|\omega|$, we recognize the phase variables $(\tilde{x}_2, \omega)$. We proceed as in Bleistein (1986) and use the method of stationary phase to integrate out the out-of-plane variable x_2 in (A1). The one-dimensional stationary phase formula approximates integrals of the type

$$\int f(\sigma) e^{\mathrm{i}\omega T(\sigma)} \mathrm{d}\sigma \approx \sqrt{\frac{2\pi}{|\omega| |\partial_\sigma^2 T(\sigma_0)|}} f(\sigma_0) e^{\mathrm{i}\omega T(\sigma_0) + \mathrm{i}(\pi/4)\mathrm{sgn}(\omega)\mathrm{sgn}(\partial_\sigma^2 T(\sigma_0))}, \quad \text{(A2)}$$

for suffi ciently large $|\omega|$ and $\partial_\sigma^2 T(\sigma_0) \neq 0$, where σ_0 is the stationary point, such that $\partial_\sigma T(\sigma)|_{\sigma=\sigma_0} = 0$. In the mentioned integral, the stationary point is given by

$$\partial_{x_2} T(\boldsymbol{x}^r, \boldsymbol{x}, \boldsymbol{x}^s) = p_2^s + p_2^r = 0. \quad \text{(A3)}$$

Due to assumptions 1 and 2, the only solution to (A3) is $p_2^s = p_2^r = 0$ which implies that the stationary point is $x_2 = 0$. A discussion on this is given in the main text. Observe that the sum of the slownesses in equation (A3) also occurs in the common azimuth case, equation (18). The second derivative of the phase function at the stationary point is

$$\partial_{x_2}^2 T(\boldsymbol{x}^r, \boldsymbol{x}, \boldsymbol{x}^s)\big|_{x_2=0, p_2=0} = (\partial_{x_2} p_2^s + \partial_{x_2} p_2^r)|_{x_2=0, p_2=0} = \frac{1}{Q_2^\perp(\boldsymbol{x}, \boldsymbol{x}^s)} + \frac{1}{Q_2^\perp(\boldsymbol{x}, \boldsymbol{x}^r)}, \quad \text{(A4)}$$

where $Q_2^\perp(\boldsymbol{x}, \boldsymbol{x}^s)$ and $Q_2^\perp(\boldsymbol{x}, \boldsymbol{x}^r)$ are the out-of-plane geometrical spreading factors defi ned in equation (5) for the rays connecting the imaging point $\boldsymbol{x}$ with the source $\boldsymbol{x}^s$ and receiver $\boldsymbol{x}^r$, respectively.

Remark 4.
In points, in phase space, where either $Q_2^\perp(\boldsymbol{x}, \boldsymbol{x}^s)$ or $Q_2^\perp(\boldsymbol{x}, \boldsymbol{x}^r)$ tends to zero the travel time function is not smooth. We observe this in equation (A4) where the Hessian of the travel time function will tend towards infinity and will not be defined. This essentially means that the stationary phase argument does not hold. The integral over x_2 in equation (A1) remains. Out-of-plane caustics are thus not allowed for the stationary phase formula to be applicable. We restrict the analysis in the following to rays with no out-of-plane caustics.

From this it follows that $\mathrm{sgn}(\partial_{x_2}^2 T(\boldsymbol{x}^r, \boldsymbol{x}, \boldsymbol{x}^s)|_{x_2=0}) = 1$ since the out-of-plane geometrical spreading is positive. The stationary phase formula (A2) then yields for the x_2 integral (in view of Remark 4)

$$\int_X \left[\omega^2 \int_{\mathbb{R}} h_m(\boldsymbol{x}^r) \rho^{(0)}(\boldsymbol{x}) A(\boldsymbol{x}^s, \boldsymbol{x}) A(\boldsymbol{x}, \boldsymbol{x}^r) \mathbf{w}^T(\boldsymbol{x}^r, \boldsymbol{x}, \boldsymbol{x}^s) \mathbf{c}^{(1)}(\boldsymbol{x}) e^{\mathrm{i}\omega T(\boldsymbol{x}^r, \boldsymbol{x}, \boldsymbol{x}^s)} h_n(\boldsymbol{x}^s) \mathrm{d}x_2 \right] \mathrm{d}x_1 \mathrm{d}x_3$$
$$\approx \sqrt{2\pi}\mathrm{i}\omega^{3/2} \int_X h_m(\boldsymbol{x}^r) \frac{(Q_2^\perp(\boldsymbol{x}, \boldsymbol{x}^s) Q_2^\perp(\boldsymbol{x}, \boldsymbol{x}^r))^{1/2}}{(Q_2^\perp(\boldsymbol{x}, \boldsymbol{x}^s) + Q_2^\perp(\boldsymbol{x}, \boldsymbol{x}^r))^{1/2}} \rho^{(0)}(\boldsymbol{x}) A(\boldsymbol{x}^s, \boldsymbol{x}) A(\boldsymbol{x}, \boldsymbol{x}^r)$$
$$\cdot \mathbf{w}^T(\boldsymbol{x}^r, \boldsymbol{x}, \boldsymbol{x}^s) \mathbf{c}^{(1)}(\boldsymbol{x}) e^{\mathrm{i}\omega T(\boldsymbol{x}^r, \boldsymbol{x}, \boldsymbol{x}^s)} h_n(\boldsymbol{x}^s)\Big|_{x_2=0, p_2=0} \mathrm{d}x_1 \mathrm{d}x_3. \quad \text{(A5)}$$

Using equation (6) this equation reduces to the 2.5-D modelling formula (9) in the main text (here in the frequency domain),

$$U_{mn}(\boldsymbol{x}^s, \boldsymbol{x}^r, \omega) = \sqrt{2\pi}\mathrm{i}\omega^{3/2} \int_X h_m(\boldsymbol{x}^r) \rho^{(0)}(\boldsymbol{x}) \frac{A^{||}(\boldsymbol{x}^s, \boldsymbol{x}) A^{||}(\boldsymbol{x}, \boldsymbol{x}^r)}{\mathcal{L}^\perp(\boldsymbol{x}^r, \boldsymbol{x}, \boldsymbol{x}^s)} \mathbf{w}^T(\boldsymbol{x}^r, \boldsymbol{x}, \boldsymbol{x}^s) \mathbf{c}^{(1)}(\boldsymbol{x}) e^{\mathrm{i}\omega T(\boldsymbol{x}^r, \boldsymbol{x}, \boldsymbol{x}^s)} h_n(\boldsymbol{x}^s) \mathrm{d}\boldsymbol{x}. \quad \text{(A6)}$$